UNCLASSIFIED

AD 403 892

Reproduced
by the

DEFENSE DOCUMENTATION CENTER

FOR

SCIENTIFIC AND TECHNICAL INFORMATION

CAMERON STATION, ALEXANDRIA, VIRGINIA

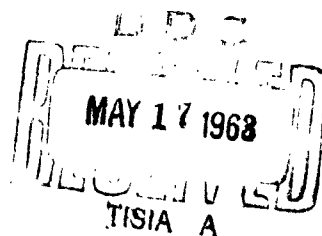# UNCLASSIFIED

403 892

INVESTIGATION OF THE STRUCTURAL AND MAGNETIC PROPERTIES OF THIN FERROMAGNETIC FILMS

TECHNICAL REPORT NO WADD TR 60-787

PART II

March 1963

Directorate of Materials and Processes
Aeronautical Systems Division
Air Force Systems Command
Wright-Patterson Air Force Base, Ohio

MAY 17 1963

TISIA A

Project No. 7371, Task No. 737103

Best
Available
Copy

NOTICES

B

ABSTRACT

Permalloy films evaporated at normal and oblique incidence to a substrate were examined by replication of their surfaces. Electron micrographs revealed chains of particles perpendicular to the incident beam when the angle of incidence was $<70°$ and parallel to the incident beam when the angle was $>70°$. The degree of alignment depended upon the angle of incidence and thickness of the film. A statistical analysis of the micrographs was made.

Permalloy films were epitaxially grown on NaCl and were annealed by electron bombardment in an electron microscope. Perfect single crystal diffraction patterns indicated the presence of [100] parent crystals and [122] twin crystals. Fringe patterns observed on electron micrographs were identified by dark field microscopy and electron diffraction as being caused by platelets of twins 100-400 A thick, lying parallel to {111} planes of the parent crystal. The non-integral reflections, commonly observed in conjunction with twin reflections, were shown to be caused by double diffraction.

The angular dependence of the torque in Permalloy films has been studied. In films with h_c, the ratio of coercive force to anisotropy field, less than 0.5, the results agree very well with the formulas for magnetization reversal in an infinite cylinder. When $h_c > 0.5$, the situation appears very complex. The unidirectional hysteresis observed in this range can be understood very well if the existence of regions with negative anisotropy is assumed. Various methods of determining the anisotropy have been compared and a torque technique for measuring dispersion in both magnitude and direction developed. The anisotropy found in films as a function of the angle of incidence of the evaporation beam and the anisotropy in epitaxially grown films is reported. Finally the use of a vibrating sample magnetometer to determine the hysteretic properties of thin films is discussed.

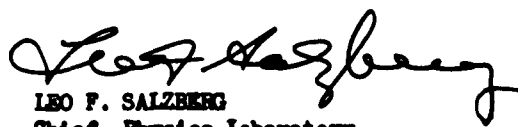This technical report has been reviewed and approved.

LEO F. SALZBERG
Chief, Physics Laboratory
Directorate of Materials & Processes

iii

TABLE OF CONTENTS

LIST OF FIGURES

THE STRUCTURAL AND MAGNETIC PROPERTIES OF THIN MAGNETIC FILMS

I. INTRODUCTION

The principle goals of this research on thin films have been A) to study their structural and magnetic properties, B) to determine the relationship between their structural properties and their magnetic anisotropy.

The structural investigation, which was carried out using electron microscopy and electron diffraction, consisted of two major phases. The first phase was a detailed study of the surface roughness of polycrystalline Permalloy and iron films, as a function of evaporation conditions, and, in particular, of the angle which the incident beam made with the substrate. The second phase involved the investigation of the defect structure of Permalloy films grown epitaxially in both high vacuum and ultra-high vacuum.

The magnetic investigation, to a large extent, was devoted to determining the nature of the anisotropy and the magnetization reversal process in Permalloy films from a study of torque behavior and rotational hysteresis. The anisotropy in Permalloy and iron films as a function of the angle of incidence was a particular area of concentration. The existence of dispersion in both magnitude and direction in Permalloy films and methods of measuring it were investigated extensively. The anisotropy in expitaxially grown films was determined, and, in several cases, both crystalline and induced anisotropy were found. Finally some work was devoted to adapting a vibrating sample magnetometer for the measurement of the hysteretic properties of thin films.

Correlations between the structural and magnetic properties have been found in three cases. These are in films evaporated at large angles of incidence, epitaxially grown films, and in films prepared from special crucible materials.

All these topics will be discussed in detail in the report below.

II. STRUCTURAL PROPERTIES

A) SURFACE STUDY OF PERMALLOY FILMS

EXPERIMENTAL DETAILS

a) Preparation of Permalloy Films:

Permalloy films were prepared by evaporating a 17 wt% Fe - 83 wt% Ni alloy from an aluminum oxide covered tungsten basket. The substrates were glass micro-cover-slides which in most instances were carbon coated to assure better release of the evaporated films. These glass slides were either kept at room temperature or heated to 70°C or 300°C during evaporation. The metal was evaporated at normal and oblique incidence with respect to the substrate. The angles were chosen arbitrarily. Before evaporation the apparatus was baked out at 200°C for 1 to 2 hours under vacuum. During evaporation the pressure remained at 5×10^{-6} mm Hg. The metal itself was thoroughly de-gassed before the magnetic shutter, placed between the source and the

target, was removed and the actual evaporation was begun. The evaporated film thickness ranged from < 100 Å to approximately 2100 Å.

b) Preparation of Replicas

Freshly prepared Permalloy films were replicated by evaporating a layer of carbon approximately 200 – 300 Å thick perpendicularly onto the surface of the Permalloy. The carbon replica was formed by the usual electron microscopical method, described by Bradley[1], of evaporation from pointed electrodes of spectrographically pure graphite; to release the replicas a solution of 50% concentrated HCl in distilled water was placed in a Petri culture dish. The glass cover slide bearing the metal film and the carbon replica was placed gently onto the surface of the acid, with the film and the replica facing upward. The surface tension of the acid solution was sufficient to cause wetting of the film-replica surface, with a subsequent dissolution of the Permalloy taking place. It was found to be advantageous to score a line around the area of the Permalloy film before placing the cover slide onto the acid. This action facilitated the dissolution of the Permalloy by permitting the acid to attack the metal more rapidly.

After the bulk of the Permalloy had obviously been dissolved, the carbon replica was freed from the cover slide by pressing gently on the corners of the slide with a needle. The carbon replica would then float free, and the cover slide would sink to the bottom of the Petri dish.

The carbon replica was permitted to float on the surface of the acid for at least one additional hour to insure that any microscopic particles of Permalloy had an opportunity to dissolve. The replica was subsequently washed on several changes of distilled water.

The replica was then broken into pieces of a size suitable for electron microscope specimens by touching it gently with a sharpened dissecting needle. The replica pieces were picked up on copper specimen screens and permitted to dry in a dessicator.

After drying, the mounted pieces of replica were then vacuum shadowed at an angle of 30° – 45°, whereupon they were ready for examination in the electron microscope.

The slides which were not previously carbon coated were handled identically. The replicas produced on these slides were much more difficult to release than the ones which had an underlying layer of carbon.

In an effort to rule out the presence of artifacts which might be misinterpreted as genuine Permalloy structure, various combinations of replicating and shadowing materials were used (Table I.)

2

TABLE I
REPLICA MATERIAL VS. SHADOWING MATERIAL

Replica material	Shadowing metal
Carbon	Platinum
Carbon	Platinum-Palladium
Carbon	Chromium
Carbon	Tungsten Oxide
Silicon monoxide	Platinum
Silicon monoxide	Platinum-Palladium
Silicon monoxide	Chromium
Silicon monoxide	Tungsten Oxide

Pt, Pt-Pd, and Cr had the tendency to agglomerate to one degree or another in the electron beam. The WO_3 was definitely superior to any other material employed. The structure exhibited by replicas of WO_3-shadowed carbon were identical to WO_3-shadowed SiO. Carbon was chosen as the replicating material because it was easier to use than SiO.

It was feared initially that the carbon replica might possibly adhere to the carbon coating of the cover slide after dissolution of the Permalloy, and thereby introduce extraneous structure into the specimen. However, it was found that this adherence of the carbon films occurred only occasionally, and when it did happen, it was easily detected both with the naked eye and in the electron microscope. When the underlying carbon film was allowed to age for several days before the Permalloy was evaporated onto it, the subsequent release of the replica was much more easily achieved since it was then virtually impossible to bring about the release of that carbon coating.

As already mentioned previously it was considerably more difficult to release the replicas when the underlying glass substrate was not coated with a carbon layer. Therefore, the majority of films were prepared on carbon covered micro-cover-slides. In addition, the fact that from time to time, the replicas would inexplicably resist any effort to bring about their release, even from carbon coated glass slides, stands as a discomfiting reminder that this entire technique is still more an art than a science. This was especially true for films which were evaporated at oblique incidence to the substrate.

RESULTS

Surface replicas taken of Fe-Ni films prepared by evaporating the metal perpendicular to the substrate exhibited in the electron microscope a structure resembling that of cobblestone pavement. The dimensions of the roughness could be calculated by assuming a simple sinusoidal variation of the thickness of the metal film. The amplitude, A, of the roughness is related to the angle of the shadow casting, α, the period, p, and the length, s, of the shadow. Using the abbreviation $t = 2\pi s/p$ the amplitude is

$$A = p(\tan \alpha) \ (2 + 2t \sin t - 2 \cos t + t^2)^{1/2}/2\pi(1-\cos t).$$

3

The measured values of $\alpha = 30°$, $p = 130$ Å and $s = 45$ Å gave $A = 24$ Å. It may, therefore, be estimated that the hills on the surface occur on the average at a separation of 130 Å and have a height of 50 Å.

The surface roughness could lead to a uniaxial magnetic anisotropy if the hills would merge into ridges along a preferred direction or would be elongated in such a direction. However, the normal incidence films exhibited generally a random orientation of the surface roughness (Fig. 1), and an occasional oriented structure which was observed (Fig. 2) remains an inexplicable exception. In order to see an alignment, the micrographs had to be examined very carefully, and even then the chains of particles did not run in a particular direction, but, rather, clusters of chains were observed running in one direction in one area and in another direction in another area. This type of alignment will be referred to as "regional alignment". It was also found that when more than one film was prepared during an evaporation, some of them exhibited a "regional alignment", while others were randomly oriented.

For films evaporated at oblique incidence to the substrate, the degree of alignment was dependent upon the angle of incidence and the thickness of the films. Thickness of the films was by far more influential than the angle of incidence. One could observe a better alignment of particle chains in thin films evaporated at a smaller angle of incidence than in thick films evaporated at a larger angle. Directional alignment of 100 Å films evaporated at 55° was rather obvious (Fig. 3). The chains of particles run perpendicular to the incident beam, as has been observed by Smith[2] and König[3], and have an average particle size of approximately 200 – 250 Å. As can be seen from the micrograph the replica was shadowed in the direction of the vapor stream of the Permalloy, making the shadow run approximately perpendicular to the particle chains. In order to rule out any artifacts which might be introduced by the direction of the shadow, the replicas were shadowed from various angles. The alignment of particles always was in the same direction, i.e., perpendicular to the Permalloy vapor stream. However, the greatest contrast was achieved when the replicas were shadowed in the same direction in which the Permalloy was evaporated. It was observed that the particle size decreases with increasing film thickness. Films 250 Å thick evaporated at 60° exhibited an average particle size of approximately 100 – 150 Å. Chains of aligned particles, however, much shorter than the ones observed in the 100 Å films, could be seen (Fig. 4).

The tendency of Permalloy films to become smoother with thickness was evident on films evaporated to 850 Å thickness at 40° incidence. Here an alignment of chains of particles which are very short can be observed (Fig. 5). As for the normal incidence films, in which an alignment of topography was present, these films also exhibited a "regional alignment".

All these films, as mentioned previously, exhibited an alignment of particle chains which was perpendicular to the Permalloy vapor stream. However, when the metal was evaporated at an angle > 70° to a substrate, a 90° reversal of the chain direction took place, i.e. the alignment was now parallel to the vapor stream. Figure 6 shows a micrograph of a film, evaporated at grazing incidence (85° – 88°), which not only shows the direction of the particle chains but also exhibits a "smearing out" of the particles in the direction of the vapor stream; similar effects were observed in all of these films.

4
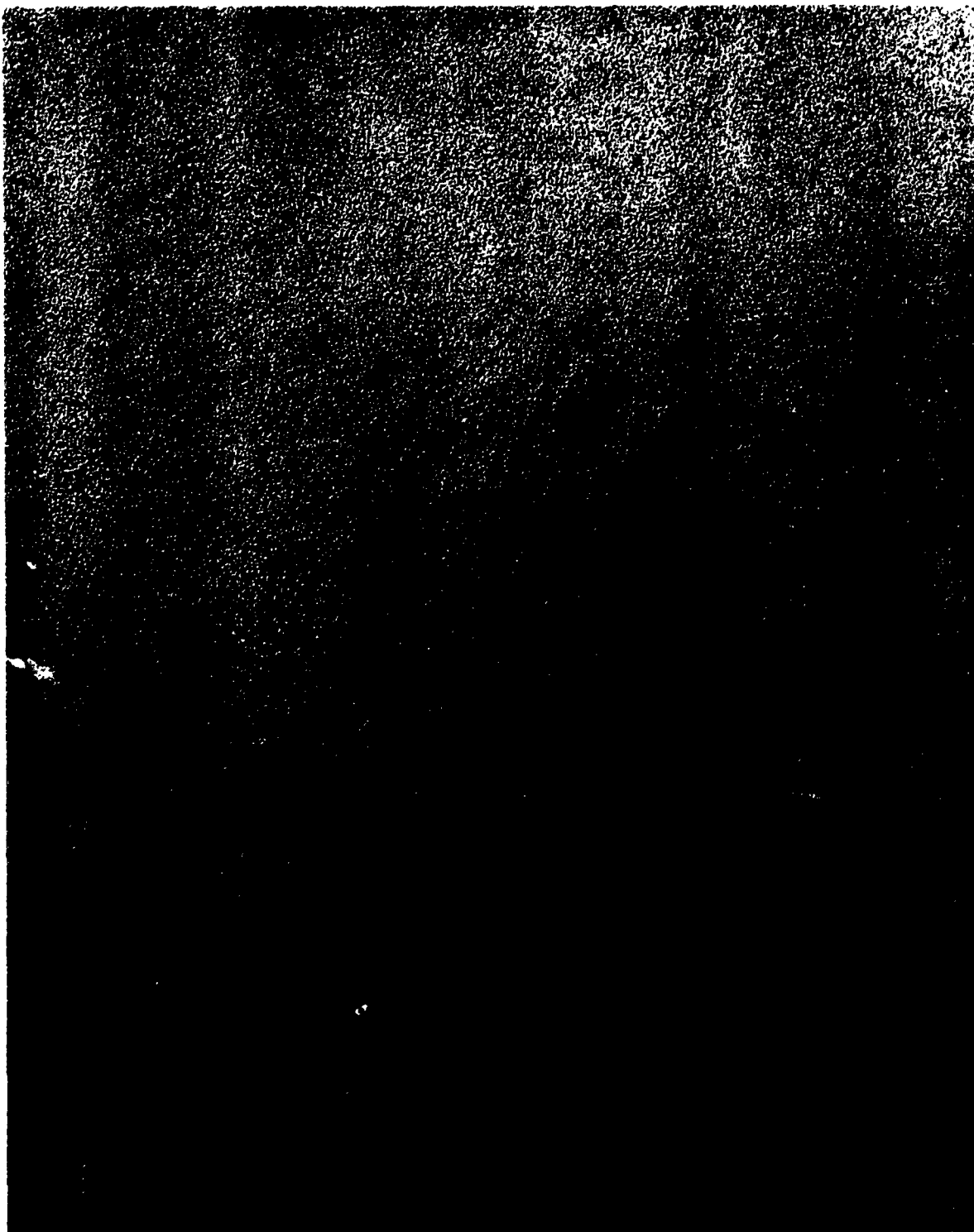
Figure 1. Electron Micrograph of Normal Incidence Film. Mag. 30,000X

Figure 2. Electron Micrograph of Normal Incidence Film Exhibiting "regional" Alignment. Mag. 30,000X

6
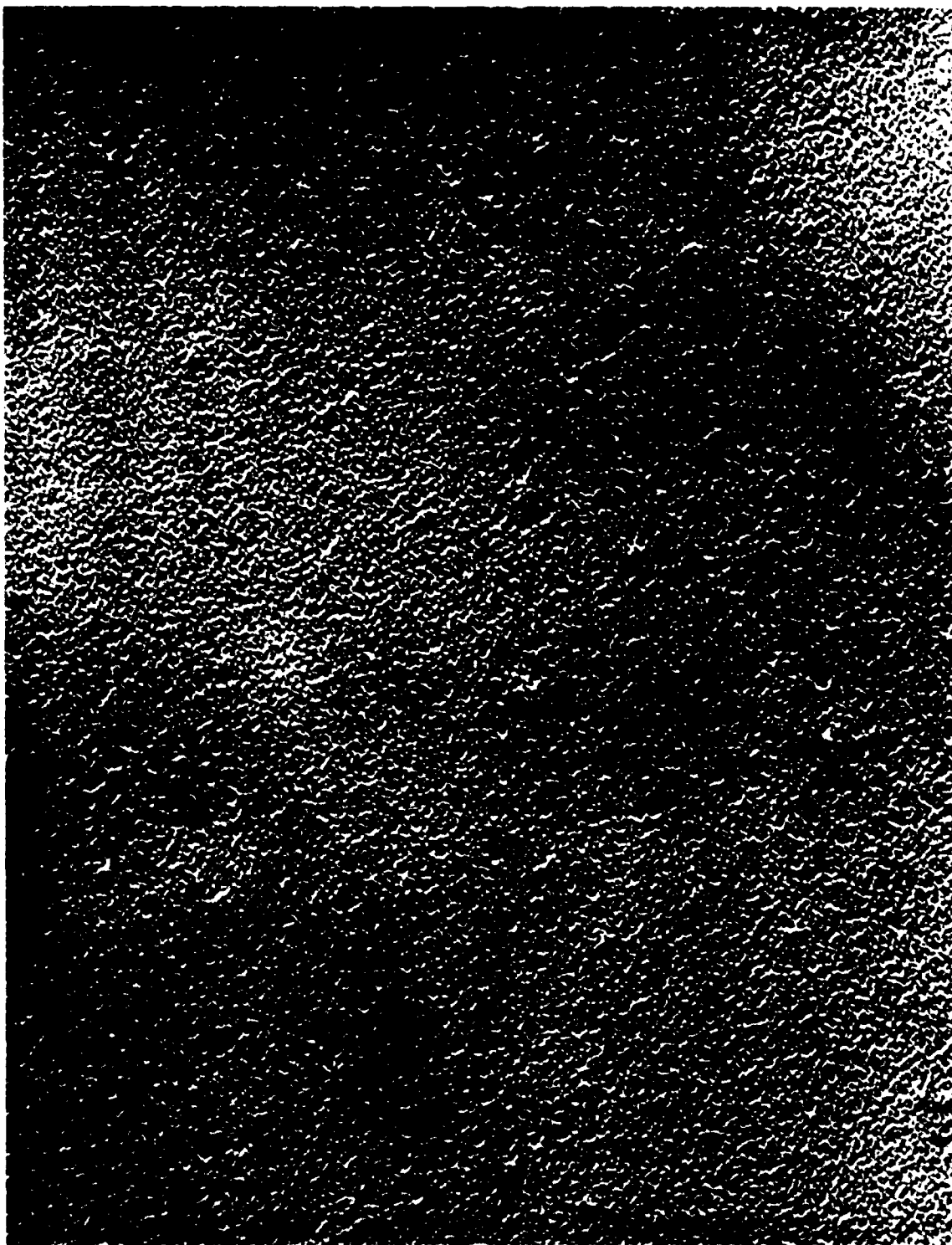
Figure 3. Electron Micrograph of Film Evaporated at 55°, 100Å Thick.
Mag. 30,000X

7.
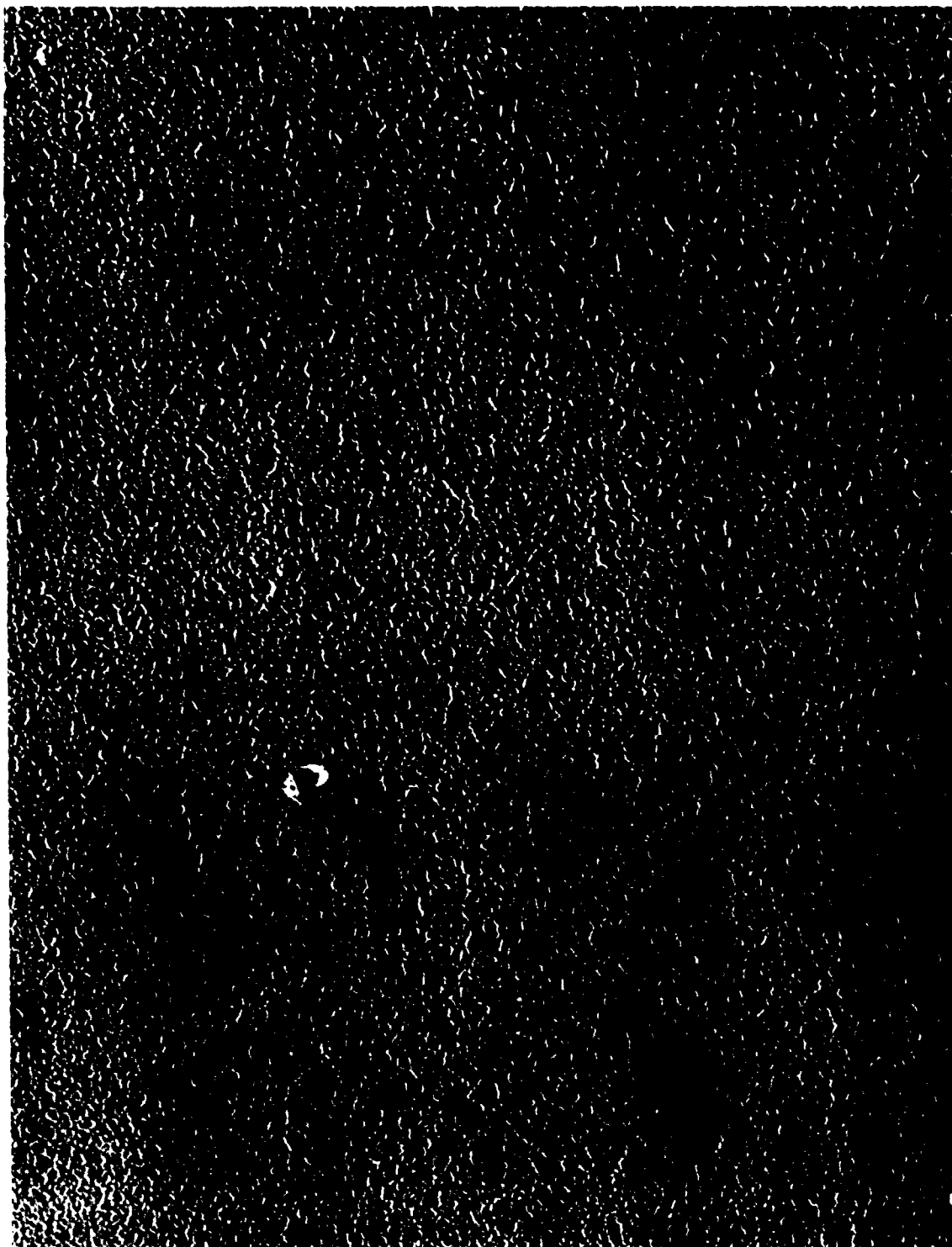
Figure 4 - Electron micrograph of film evaporated at 60°, 250Å thick. Mag. 30,000X

8
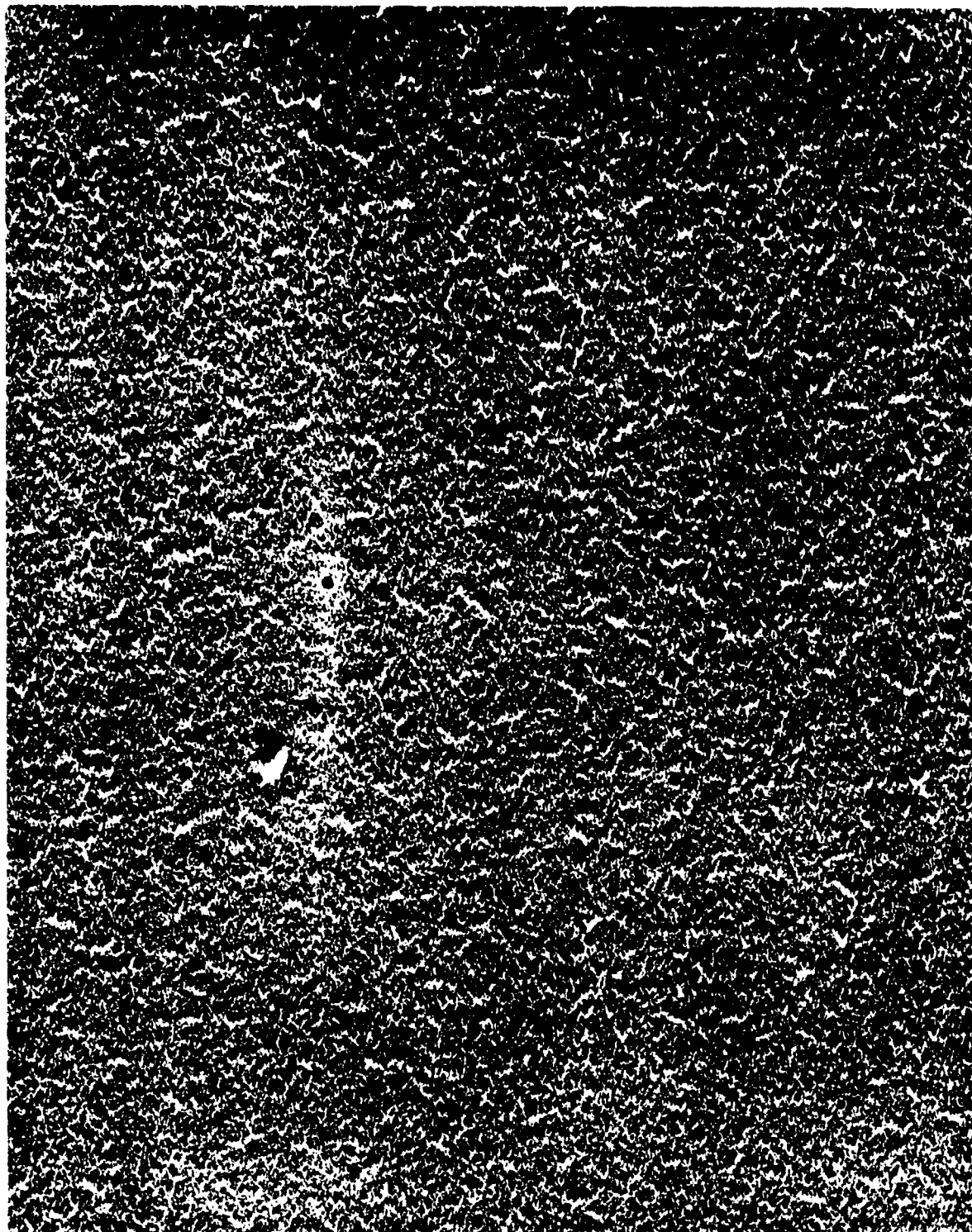
Figure 5 - Electron micrograph of film evaporated at 4C°, 850Å thick. Mag. 36,000X

Figure 6 - Electron micrograph of film evaporated at 85°, 500Å thick. Mag. 30,000X

In an attempt to secure quantitative data, a statistical count of chain directions was made. Any chain with more than two particles adjacent to each other was counted for this purpose. A total count of approximately 800 chains for each micrograph was made. This data was plotted as degree θ vs frequency of direction in % (Fig. 7). The direction of the shadow casting was taken as 0°. From these graphs it can be shown that the thin films (100 Å) have a very high uniaxial peak (Fig. 7c). The 250 Å film (Fig. 7d) also exhibited a uniaxial tendency. So, one can conclude that an alignment of surface topography is rather evident for films up to 250 Å thick. For thicker films and smaller angles of incidence the graphs show a more and more randomly oriented pattern, as predicted by visual inspection of the micrographs (Fig. 7e). It is also evident that there is a directional trend in the few films evaporated at normal incidence for which this trend was predicted (Fig. 7b).

CONCLUSION

It can therefore be concluded that normal incidence Fe-Ni films in general do not exhibit a preferred surface orientation. Films evaporated at various angles of incidence have surface alignment, the degree of which depends on the angle of evaporation and the thickness of the films. The cleaning method of the substrates is very influential on the final films. After the substrates have been cleaned, it is of utmost importance to place them into the evaporator immediately.

B. STUDY OF EPITAXIALLY GROWN PERMALLOY FILMS

a) Experimental Technique

The films were prepared by evaporation of zone-refined Permalloy (83% wt Ni, 17% wt Fe) onto the cleavage face of a heated NaCl crystal. The experimental details were quite similar to those described by Burbank and Heidenreich[4], except that the films were floated off the substrate without being reinforced by a plastic lacquer. The films were 600-800 Å thick, as measured by optical interferometry of control specimens made on glass slides. The annealing was done in the electron microscope by increasing the electron current for a few seconds to a value at which the Permalloy and the copper supporting grid would melt after prolonged bombardment. This led to a sintering of the pseudo monocrystalline film into relative large areas of film, extending over several grid openings and giving perfect single crystal diffraction patterns without any trace of polycrystalline components.

Electron diffraction, dark-and bright-field electron microscopy and selected area diffraction was done with the RCA electron microscope using the diffraction attachment for diffraction work. The instrument was operated at 100 KV. For some of the dark-field photographs the alignment of the instrument was changed in order to have the diffracted beam passing as close to the optical axis of the instrument as possible. The influence of specimen rotation and beam divergence was tested, the latter by defocussing the double condenser. While rotation of the specimen had a pronounced effect, the results were largely independent of the particular setting of the condenser.
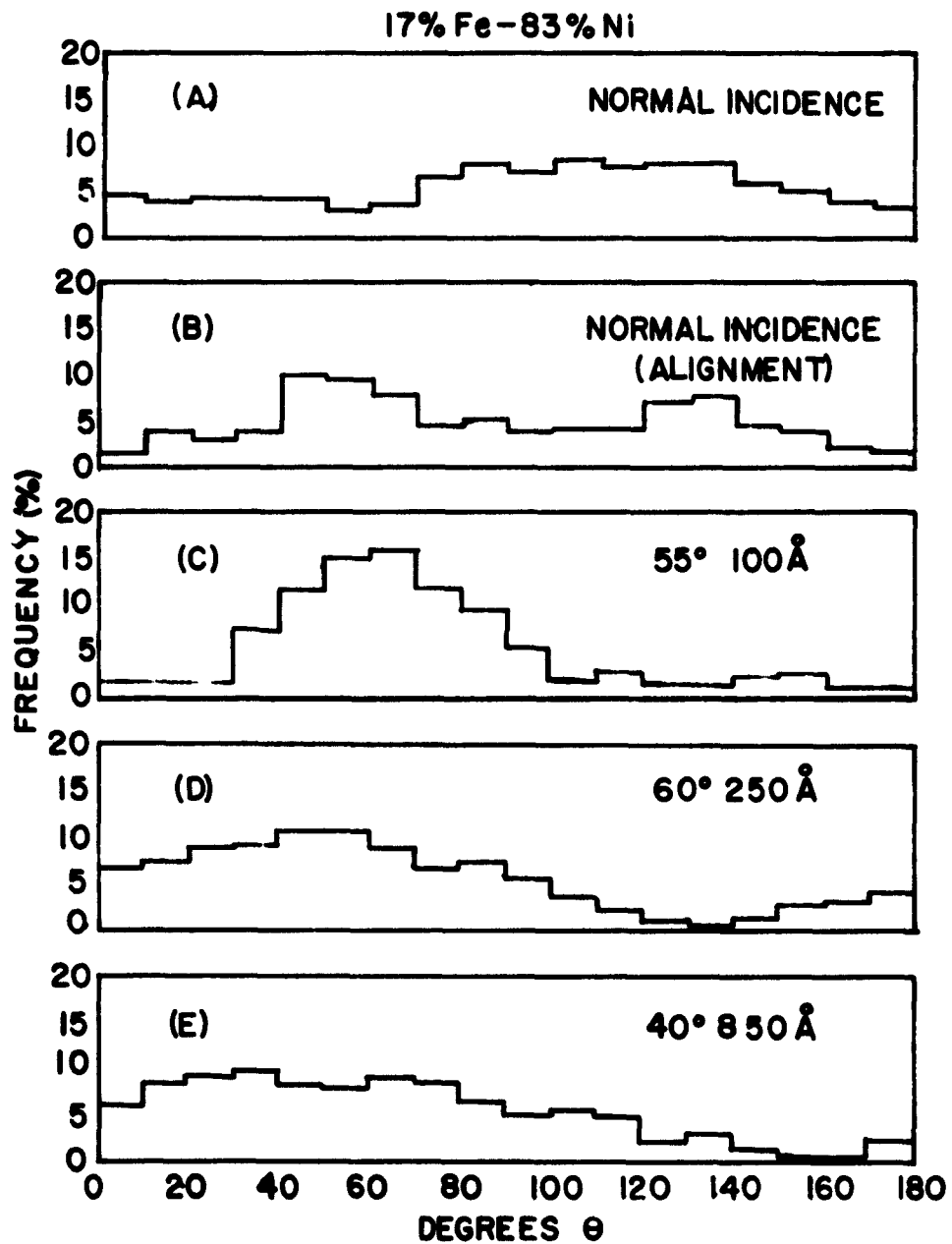
Fig. 7 - Graph of statistical count of chain directions.

12

b) Electron Diffraction Results

The diffraction patterns obtained with unannealed, pseudo monocrystalline films were very similar to that shown in Burbank and Heidenreich's[4] paper. Spot reflections were superimposed on rings if they originated from the parent lattice with a [100] orientation or from (111) twins of that lattice. In addition, non-integral spots and streaks joining the twin and parent reflections were observed.

After annealing, good spot patterns were obtained containing parent, twin and non-integral reflections. By rotating the specimen around an axis perpendicular to the electron beam, the appearance and disappearance of the parent and twin reflections was investigated. This followed a pattern which could easily be predicted by reciprocal lattice considerations assuming the superposition of one [100] parent lattice and four [122] twin lattices.

The behavior of the non-integral reflections was of particular interest because they would appear and disappear together with their corresponding twin reflections if they were due to double diffraction. Figures 8a and 8b show that this is the case. After rotation of the specimen by 5°, strong twin reflections appeared above and below the central beam. At the same time non-integral reflections show up above and below the two strong parent reflections to the left and right of the central beam. This finding supports the view held by Thirsk and Whitmore[5], Göttsche[6] and Burbank and Heidenreich[4] that the non-integral reflections are mainly due to double diffraction. The numerous non-integral reflections observed on other diffraction patterns could all be explained, in a qualitative manner, by double diffraction from the parent crystal and its twins. A quantitative comparison of the reflected intensities was, however, not possible because the direct beam and the strong beam, which is reflected by the parent crystal and gives rise to the non-integral reflections by being diffracted again by the twins, traverse the twins in different directions.

In addition to the non-integral reflections, streaks extending in the <111> directions and joining parent and twin reflections were observed. Their explanation has been given by Göttsche[7] in terms of diffraction from a lattice containing one-dimensional faults. These streaks were more pronounced in unannealed films, indicating a higher faulting probability for these specimens. Figure 9 shows streaks on a selected area diffraction pattern of an unannealed film.

If the twinned material would occur in very thin lamellae, parallel to {111} planes, causing essentially two-dimensional diffraction, the reciprocal lattice points would degenerate into rods extending in the <111> directions. However, the appearance of the twin reflections on the photographs and their behavior during rotation of the specimen showed that the reciprocal lattice of the twins is essentially a point lattice, suggesting that the twinned regions are thick enough to give three dimensional diffraction effects. This finding excludes the interpretation that the twin reflections are due to extrinsic stacking faults, the thinnest twins possible.

13
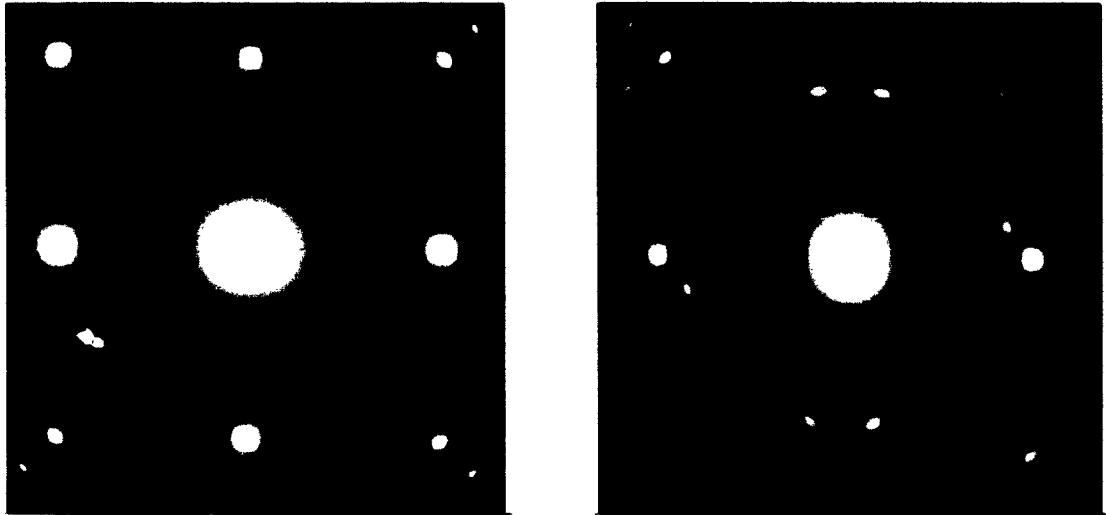
Fig. 8 - Electron diffraction pattern of an annealed Permalloy film before and after rotation of the specimen by 5° about an axis perpendicular to the beam. The simultaneous appearance of twin plus non-integral reflections suggests that the latter are due to double diffraction.
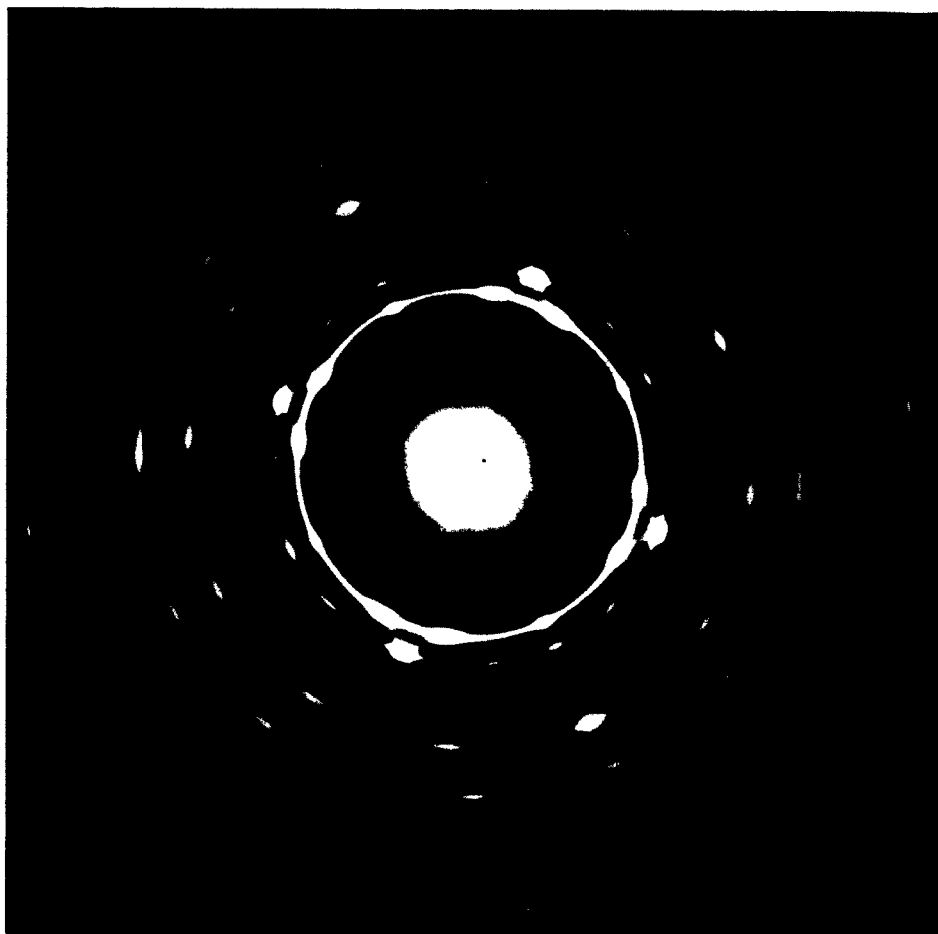
Fig. 9 - Selected area diffraction of an unannealed film showing streaks caused by faulting.

c) Electron Microscopy Results

Electron micrographs of the unannealed films were similar to those shown by Burbank and Heidenreich[4]. Micrographs of the annealed specimens showed considerably more details, allowing a correlation between diffraction effects and image appearance. The micrograph reproduced in Figure 10 shows numerous faults which extend in the [110] direction. From the thickness of the film and the width of the faults on the micrographs it was estimated that the faults could be platelets lying in the {111} planes and intersecting the film surface in <110> directions.

The appearance of some of the faults might suggest that they are stacking faults, Matthews[8], Phillips[9]. However, dark-field photographs taken with the twin reflections always showed the faults in contrast. Moreover, these faults were the only regions which contributed to the twin reflections. It may, therefore, be concluded that twinning causes the fault contrast seen on the micrographs. Figure 11 (a,c) shows that the intensity diffracted into the chosen twin reflection is due to fringes of only those faults which extend from left to right in the figure. Similar micrographs were taken using all twin and non-integral reflections surrounding the 200 reflections of the parent lattice. The results and their interpretation are shown schematically in Figure 12.

Figure 12 is a combination of stereographic projection, reciprocal lattice, and actual crystal drawing. The square in the center represents the top surface of a [100] cube of the parent crystal. Parts of the four {111} planes are shown by shaded areas. On each of the {111} planes a twin (A, A', B, B') can be formed which is depicted as a tetrahedron with {111} faces, one of the {111} faces of the twin being in contact with a (111) face of the parent crystal. The twinning planes intersect the cube surface of the parent crystal in <110> directions which are shown as [A], [A'], [B], and [B'] on the stereographic circle around the center. Crosses on the circle represent the poles of the {100} planes of the parent crystal. The poles of the twin {111} planes are shown as open circles.

Electron diffraction diagrams of a specimen in [100] orientation look similar to the stereographic plot shown in Figure 12, except, however, that reflections corresponding to all four 200 crosses and all eight 111 open circles will not appear simultaneously because of the angular difference between the {100} parent and {111} twin planes. The figure illustrates that a dark field photo taken with the twin reflection appearing at a position marked, say A, A' will show those twins whose twinning planes intersect the specimen surface in [A], [A'] direction. All dark-field, and their corresponding bright-field, photos showed that the fringe pattern of the twins is elongated in the direction of intersection of the twinning plane with the surface.

These observations may be interpreted by making use of Figure 13. Assuming a nominal film thickness of 700 Å and a twinned region extending from top to bottom of the foil, as indicated in the left drawing in Figure 13, the top and bottom parts, W, of the twin are wedge-shaped, while the center part, U, has constant thickness in the direction of the direct beam. Still referring to the left of Figure 13, it is evident that the transmitted beam would show two extinction fringes running parallel to the line of intersection of twinning plane and surface. For the case of the drawing, the extinction distance given by Hirsch, Howie and Whelan[10] for nickel, 250 Å, has been applied to Permalloy. The intensity distribution of the transmitted beam has been indicated in the lower part of Figure 13.

16
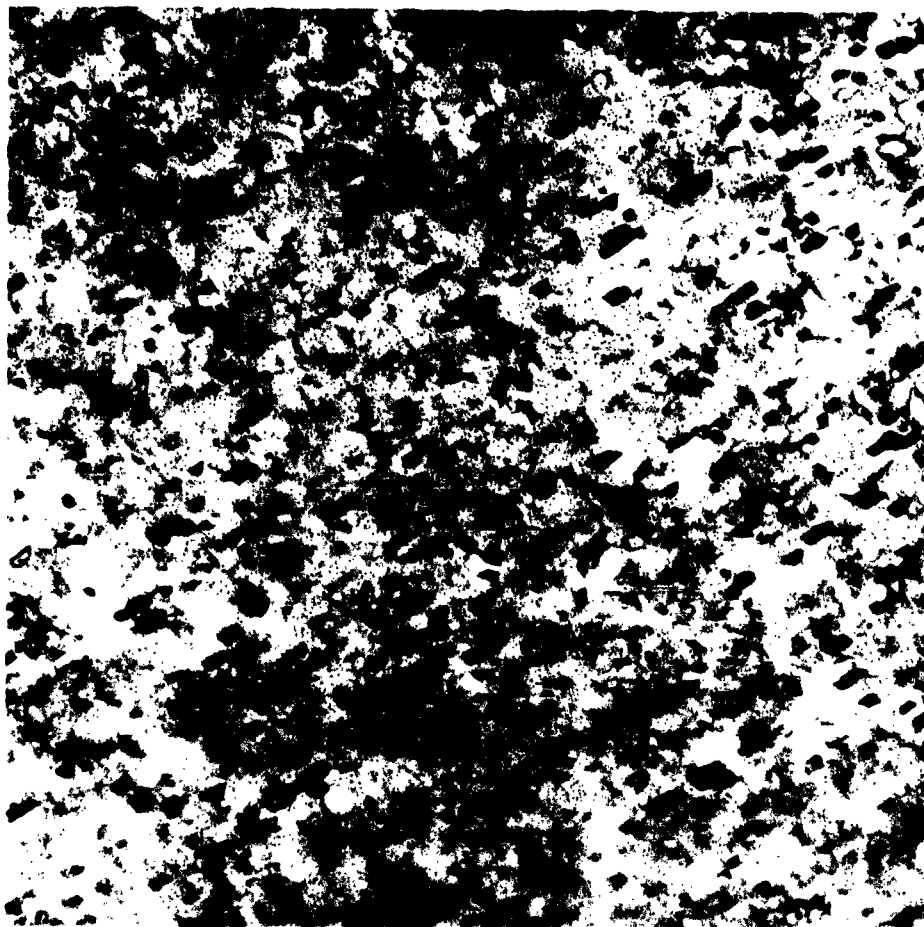
Fig. 10 - Electron micrograph of annealed film. Faults have been identified as twins.

17
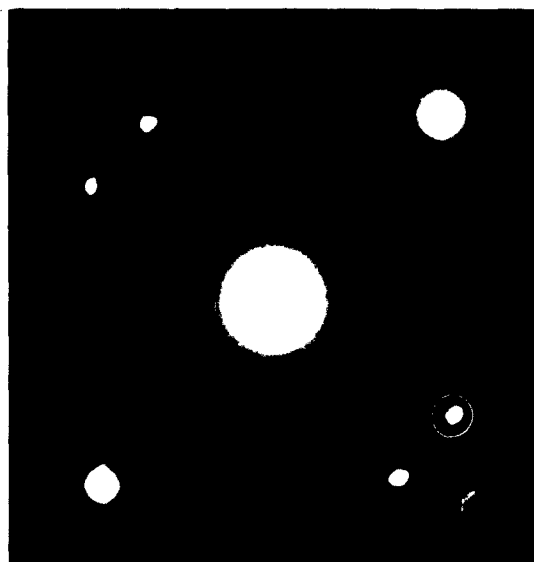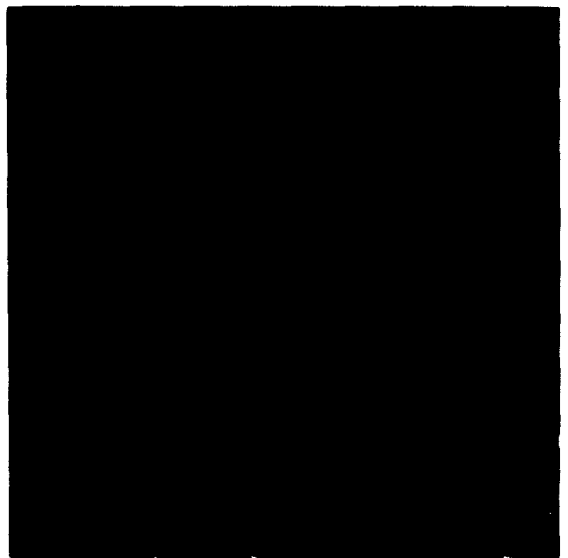
Fig. 11 - Bright field, dark field and selected area diffraction pattern of same area.
The twin reflection which has been used for the dark field photograph is
indicated by a circle. Comparing bright and dark field photographs it is
seen that only faults extending in one direction are imaged in the dark
field micrograph.

18
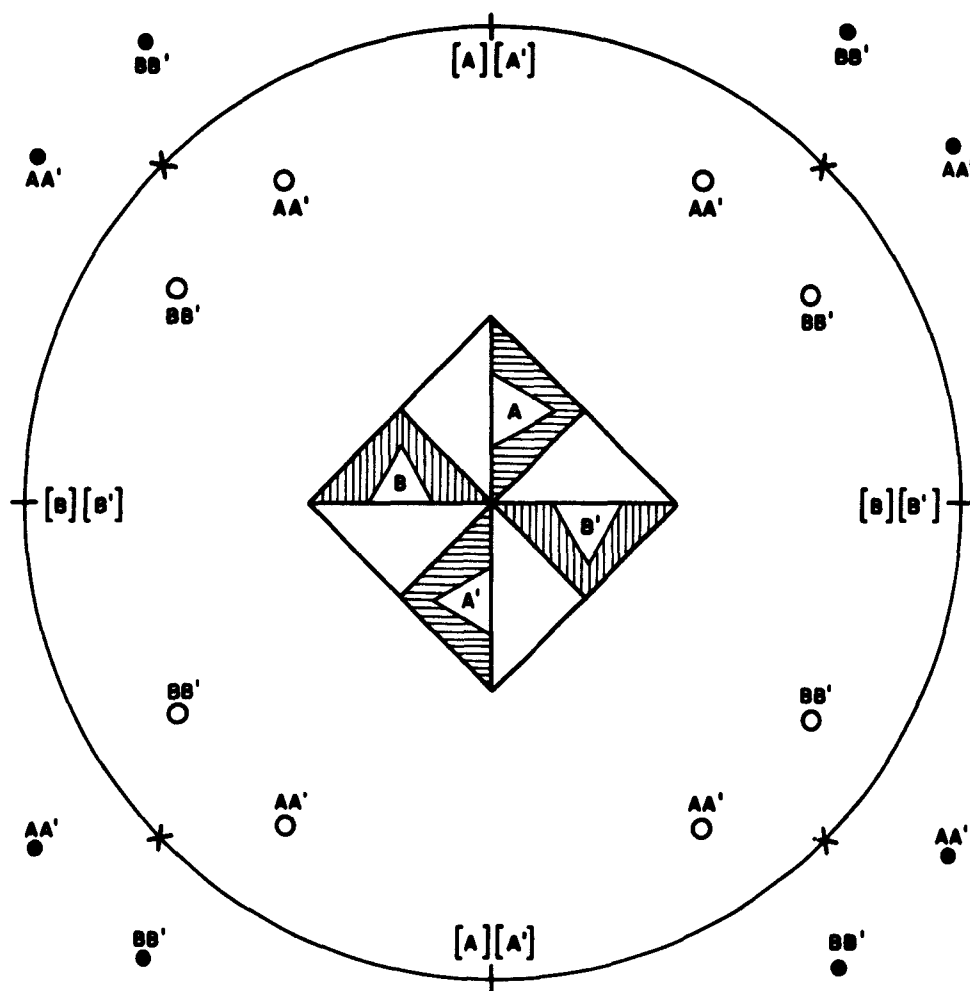
Fig. 12 - *Stereographic projection, reciprocal lattice, and actual crystal drawing.*
See text for explanation.

19
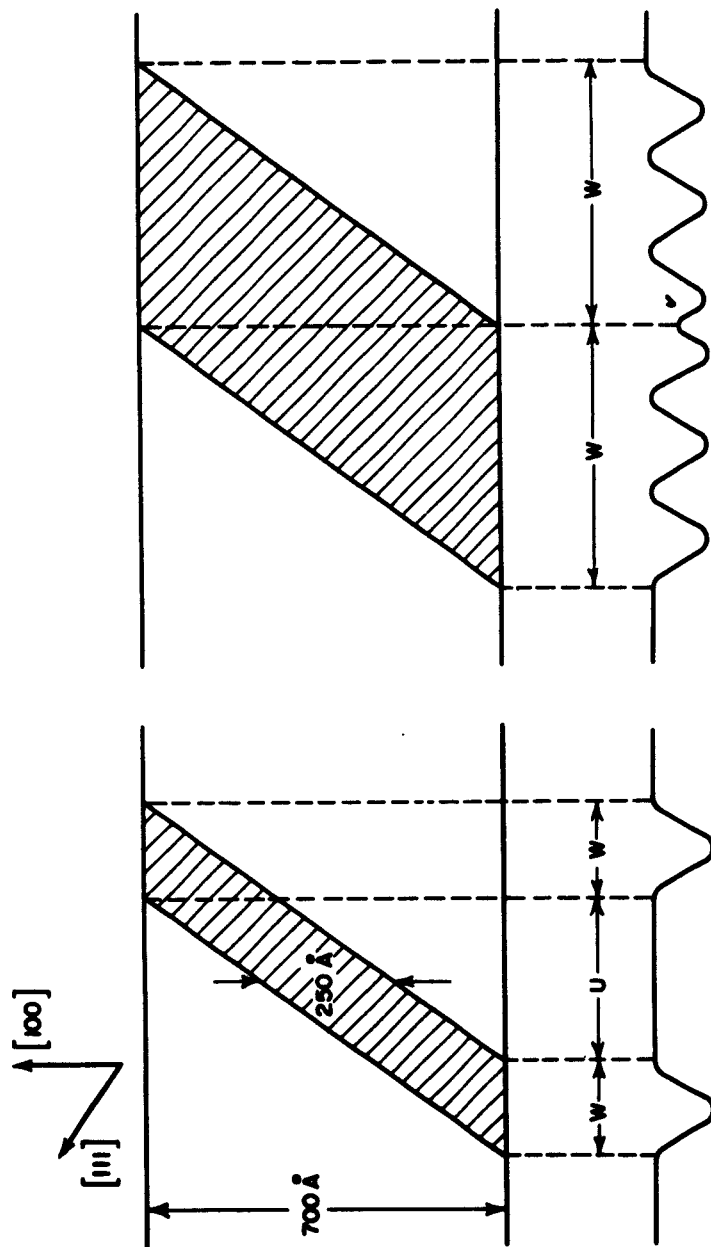
Fig. 13 - *Twinned region, shaded area, intersects 700Å thick film. Intensity distribution in the transmitted beam, indicated at the bottom, shows extinction fringes caused by wedge shaped parts (W) of the twin.*

20

For twins thicker than that in the left part of Figure 13, it may be seen from the right part of Figure 13 that a maximum of five extinction fringes, the central fringe being somewhat indistinct, could be expected. The faults shown in Figure 10 demonstrate this behavior.

In addition to the fringe pattern predicted from Figure 13, more complex fringe patterns have been observed. Figure 14 shows a dark-field potograph taken with a twin reflection. The more irregular shape of the twins is obvious. A prediction from the diffraction theory, Hirsch, Howie and Whelan[10], that the number of fringes should increase the more the specimen orientation deviates from the reflection position is also visible in Figure 14.

The explanation given here ignores the fact that the twins are surrounded by parent crystal material. Whether the parent crystal takes part in fringe formation would depend on the closeness of its orientation to a reflecting position. In general, it was observed that different areas showed up on the dark-field photographs taken with different reflections, indicating that multiple diffraction would be negligible.

Referring back to Figure 12, the full points outside the stereographic circle represent schematically the positions of the non-integral reflections. If these reflections are due to double diffraction of a strong 220 reflection by the twins, dark-field photographs taken with these reflections should show fringe patterns corresponding to the twins marked A, A', B, B' in Figure 12. This has been observed and supports the interpretation that the non-integral reflections, at least to a great extent, are due to double diffraction.

d) Conclusion

Annealing of Permalloy monocrystalline films in the electrons beam gave specimens of perfect [100] orientation containing a high percentage of (111) twins. By electron diffraction and microscopy, it was shown that the twins gave a fringe pattern which could be explained in terms of platelets lying parallel to the {111} planes of the parent crystal. The thickness of the twin platelets was estimated to vary between approximately 100 Å and 400 Å.

Diffraction and dark-field microscopy indicated that the non-integral reflections commonly observed in conjunction with twin reflections are due to double diffraction.

III. MAGNETIC PROPERTIES

A) ROTATIONAL HYSTERESIS IN PERMALLOY FILMS

1) Ratio of Coercive Force to Anisotropy Field < 0.5

Torque curves in thin Permalloy films have been studied using a high sensitivity (10^{-3} dyne-cm) continuous recording torque magnetometer[11]. The results reported here are for a 1500 Å, 77% Ni film, prepared by vacuum deposition in a magnetic field[12]. The hysteresis loop, taken at 1000 cycles, was rectangular in the easy direction with a coercive force $H_c = 1.0$ oe. In the hard direction, it was reversible with an average anisotropy field $H_K = 5.8$ oe.

21

Figure 14 - Dark field photograph with twin reflection.   Mag. 90,000X

22

The experimental results are summarized in Figures 15-17. Examples of the recorded torque curves*, all of which had a period of 180°, are shown in Figure 15. For applied fields $H < H_c$, or in the more convenient reduced field notation, $h < h_c$, where $h = H/H_k$ and $h_c = H_c/H_k$, the torque was essentially zero. For $h_c < h < 1$, the curves were irreversible, i.e. showed rotational hysteresis and were of the type shown in Figure 15 (a). For $h > 1$, the hysteresis vanished and curves similar to Figure 15 (b) were observed. This last result is in disagreement with the earlier work of Mayfield[13] who, using a different technique, reported a non-zero value of rotational hysteresis even for fields as large as $h = 15$.

The anisotropy constant K was 2.5×10^3 ergs/cc. It was determined from the magnitude of the high field torque curves which became field independent for $h > 0.9$. For $h > 6$, the curves assumed a nearly pure sine dependence.

The rotational hysteresis loss per unit volume[14] was computed from the torque curves and is plotted versus the reduced field in Figure 16.

Figure 17 shows the component of the reduced critical field in the easy direction, h_L, as a function of the component in the hard direction h_T.

The experimental results were compared with various theoretical pictures of magnetization processes in ferromagnets as shown in Figures 15-17. Three models were considered: (a) coherent rotations as described by Stoner and Wohlfarth[15]; (b) 180° wall motion in a uniaxial single crystal as discussed by Kondorsky[16]; (c) an adaptation of the results of the calculations by Shtrikman and Treves[17] on non-coherent reversal in an infinite circular cylinder.

(a) Coherent Rotation: Here the film is considered to be a single domain particle with uniaxial anisotropy. The saturation magnetization, I_s, is given by $I_s = \frac{2K}{H_k}$. Using the experimental value of H_k and K, I_s was calculated to be 860 emu/cc, which is in close agreement with the bulk value[18]. As shown in Figure 15, the reversible parts of the experimental torque curves are in very good agreement with the calculated ones. The onset of irreversible torque reversal, as well as the magnitude of the rotational hysteresis, are however, in wide disagreement with this model except in fields approaching $h = 1$.

(b) 180° Wall Motion: Here it is assumed that the hysteresis loop is rectangular and that only the component of the field parallel to the easy axis is effective. This should be a good approximation as long as the magnetization is parallel to the easy axis, i.e., for $h \ll 1$. It follows, accordingly, that the rotational hysteresis, W_r, is field independent, with a value

$$W_r = 4\,H_c\,I_s \tag{1}$$

The critical angle θ_c is given by

$$\cos = \frac{-h_c}{h} \tag{2}$$

---

*To define its magnetic history prior to measurement, the film was demagnetized in a slowly decreasing 1000 cycle field. In addition, before recording each curve, the applied field was cycled 180°.

23
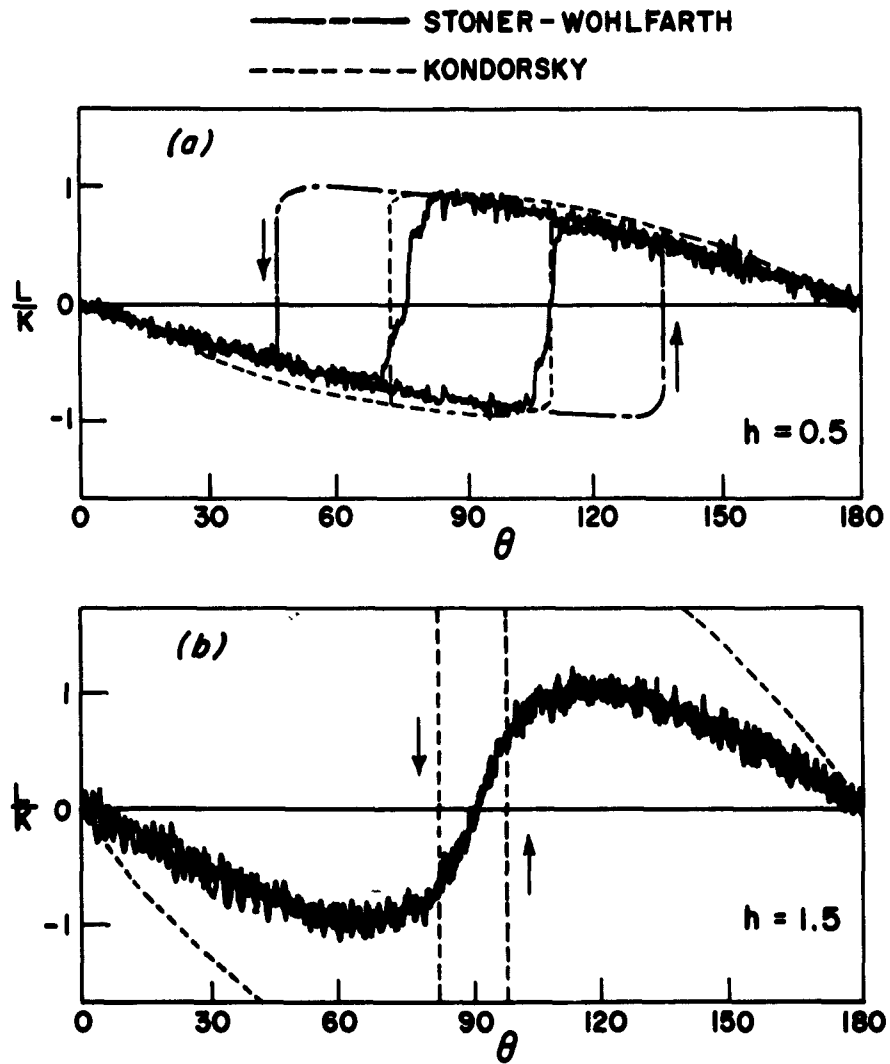
Fig. 15 - Angular dependence of the torque L, plotted in reduced units, for two values of the reduced applied field; (a) h = 0.5, (b) h = 1.5. The broken curves are those calculated from the Stoner-Wohlfarth (S-W) and Kondorsky models. Reversible portions of the (S-W) curves are not shown in both (a) and (b), since they fall on the experimental curves. Arrows indicate the direction of rotation of h.
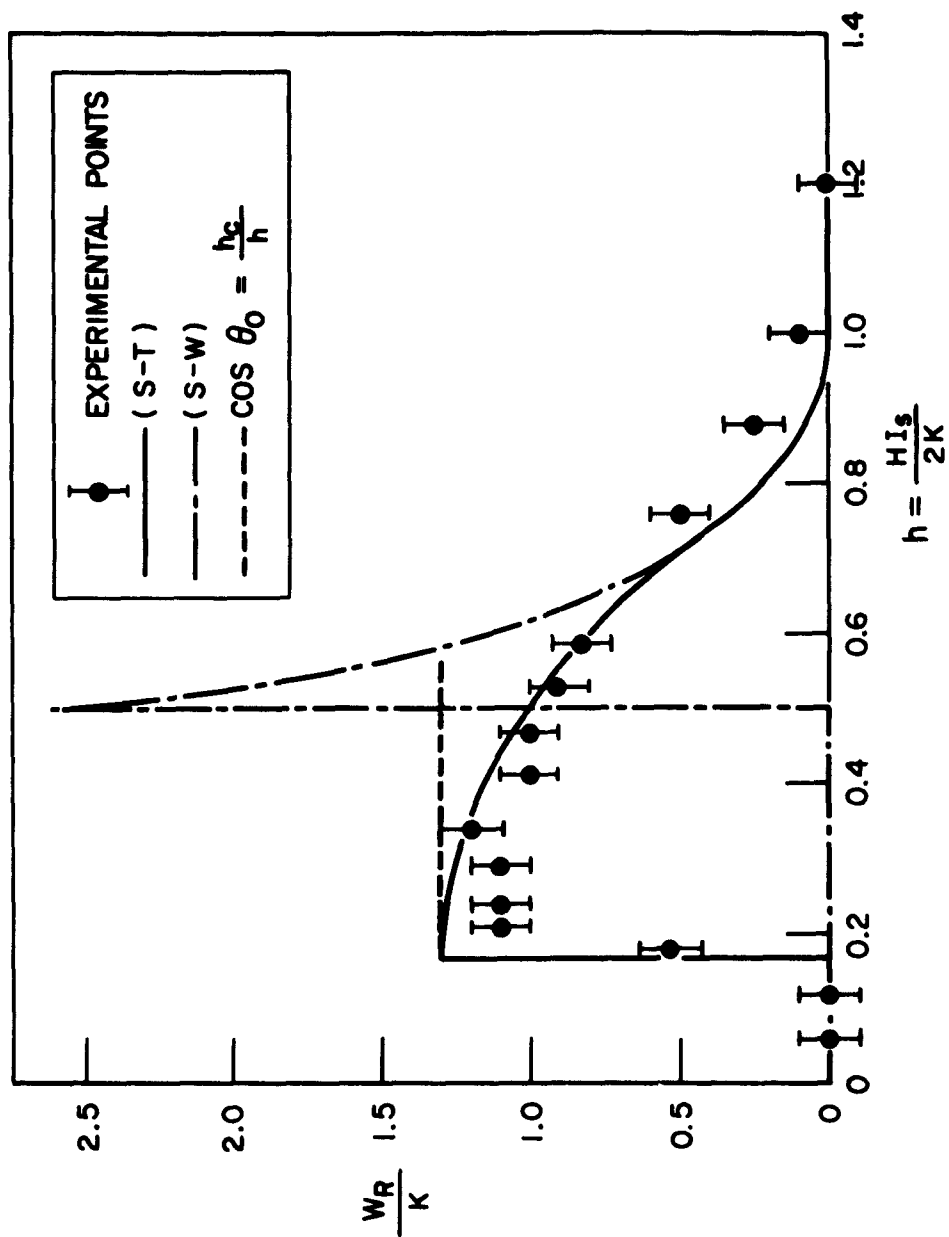
Fig. 16 - Rotational hysteresis W_r, plotted in reduced units, vs. reduced applied field. The theoretical curves are those derived from the treatments by Shtrikman and Treves (S-T), Stoner and Wohlfarth (S-W), and Kondorsky.
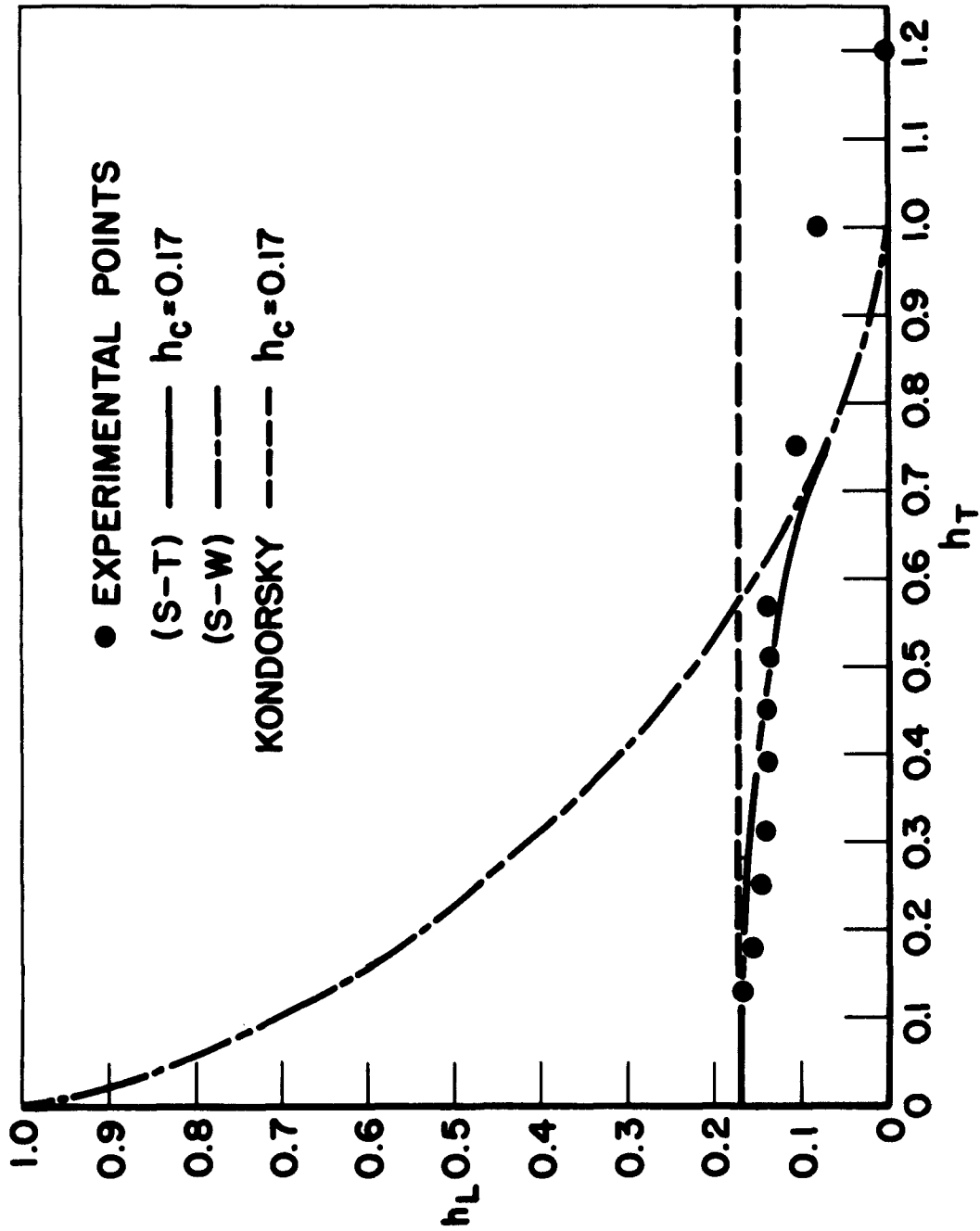
Fig. 17 - The component of the reduced critical field in the easy direction, h_L vs. the component in the hard direction, h_T. The theoretical curves are those derived from the treatments by Shtrikman and Treves (S-T), Stoner and Wohlfarth (S-W), and Kondorsky.

Since the magnetization is parallel to the easy axis, the torque L, is simply

$$L = -H \, I_s \, \text{Sin} \, \theta, \quad \theta < \theta_c$$

$$L = H \, I_s \, \text{Sin} \, \theta, \quad \theta > \theta_c \tag{3}$$

Examination of Figures 15-17 shows that for $h \ll 1$, the predictions based on this model are in good agreement with experiment. However, as h approaches 1, discrepancies appear which grow as h increases.

(3) Non-Coherent Rotation: Here the torque curves are identical to those calculated from the Stoner-Wohlfarth model except when

$$h^2 < \left(1 - 3h_c + 3h_c^2\right) \tag{4}$$

When Equation (4) is satisfied, the critical angle is given by

$$\text{Cos} \, \theta_c = \frac{-h_c}{(1-2h_c)^{1/2}} \left[\left(\frac{1-h_c}{h}\right)^2 - 1\right]^{1/2} \tag{5}$$

although in the regions where the curves are reversible, they are the same as the Stoner-Wohlfarth curves, calculated for corresponding regions.

The hysteresis losses are computed as described by Shtrikman and Treves. Comparison with experiment, Figure 16, shows that this model fits the experimental results reasonably well over the entire field range.

In order to obtain the critical switching curves in the usual form, it is convenient to rewrite Eq. 5 in terms of h_L and h_T. It then becomes

$$\left(\frac{h_L}{h_c}\right)^2 + \left(\frac{h_T}{1-h_c}\right)^2 = 1 \tag{6}$$

Figure 18 shows a plot of this function* for several values of h_c.

In Fig. 17, the experimental switching curve is shown for the particular case discussed, and the agreement with the Shtrikman-Treves model is again seen to be reasonably good.

These favorable results are in fact no surprise. For cases where $h_c \ll 1$, as for this film ($h_c = 0.17$), the model is equivalent to the Stoner-Wohlfarth one in the region $h \sim 1$ and to the Kondorsky one for $h \ll 1$. As it is hard to attach physical meaning to the picture assumed in the derivation of equation (5), i.e., an infinite circular cylinder describing a thin film, it is perhaps best to regard it an interpolation scheme between the limits of the Stoner-Wohlfarth and the Kondorsky models.

---

*The authors are indebted to Dr. E. P. Wohlfarth for suggesting the presentation of the critical switching curve in this form.
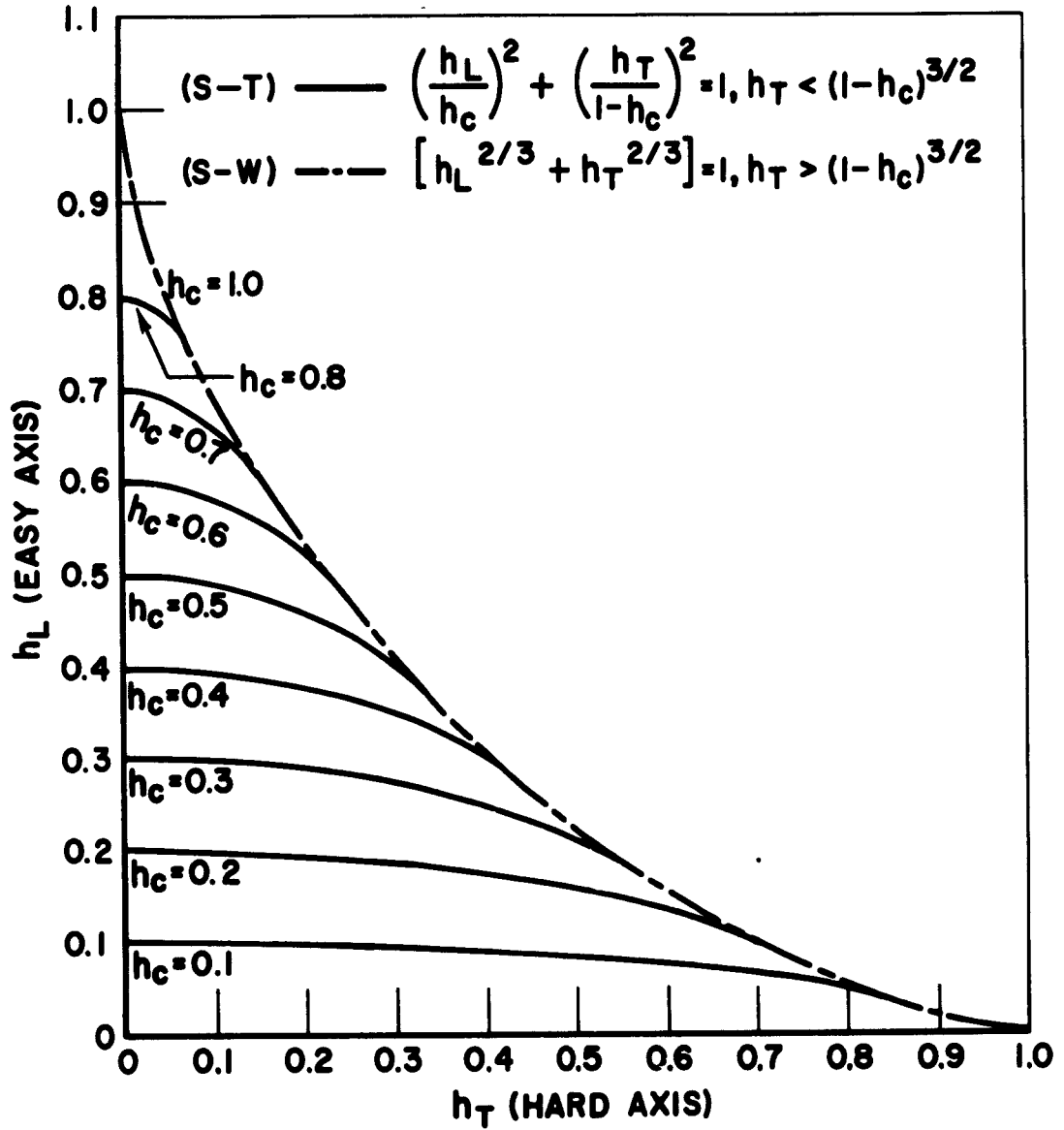
Fig. 18 - *Theoretical critical switching curves for several values of the reduced coercive force, h_c, derived from the Shtrikman and Treves (S-T) model. Also the critical curve derived from the Stoner and Wohlfarth (S-W) model, to which the (S-T) model reduces when $h_T = (1-h_c)^{3/2}$.*

As a further check on the validity of the Shtrikman-Treves model in thin films, an experimental study of the dependence of the hystertic properties on the parameter h_c was undertaken. Fig. 19 shows the results* for the maximum reduced rotational hysteresis W_r/K and the rotational hysteresis integral[19] W. For $h_c < 0.5$ the agreement between theory and experiment is satisfactory. For $h_c > 0.5$ the experimental value of W is too large. Thus, the range of applicability of the model is limited to $h_c < 0.5$. The situation in the range $h_c > 0.5$ is much more complex and is discussed in detail below.

2) Ratio of Coercive Force to Anisotropy Field > 0.5

A study of torque curves in thin Permalloy films, and the field dependence of the rotational hysteresis[14] in particular, has revealed that the results are dependent on the value of the reduced coercive force $h_c = H_c/\overline{H}_k$, where H_c is the coercive force in the easy direction and $\overline{H}_k$ is the average anisotropy field. Further, the films can be classified according to their torque curves in one of two categories, depending on whether $h_c < 0.5$ or > 0.5.

A previous section has discussed the case of $h_c < 0.5$ where both theoretically and experimentally the situation appears relatively straightforward. In that region, the results agree very well with formulas derived by Shtrikman and Treves[17] (S-T) for the magnetization reversal in an infinite cylinder.

The extension of the work to the case $h_c < 0.5$, has shown that the coherent rotation theory of Stoner and Wohlfarth[15] (S-W), to which the model reduces in this range, does not adequately describe the experimental results. This is illustrated by a typical example: a 1400 Å, 77% Permalloy film with $h_c = 0.9$. For applied fields $h < 1.5$ (Fig. 20a), using the reduced notation, the torque, as expected from (S-W), is sinusoidal with a period of π a field-independent amplitude. However, it is irreversible, as found also by Mayfield[13] and Takahashi et al[20]. For $0.7 < h < 1.5$, Fig. 20b, a well-defined uniaxial hysteresis** is observed, associated with the anisotropy of the bulk of the film. Here, the behavior is characteristic of the (S-W) model. For $0.5 < h < 0.7$ Fig. 20c, the torque is irreversible and rather irregular. For $h < 0.5$, if the film is previously saturated, the torque has a period of 2π in agreement with the (S-W) model. However, when $0.3 < h < 0.5$, it is irreversible and the hysteresis is unidirectional** occurring around the easy direction of the bulk of the film. The experimental curve in this case is shown in Fig. 21 (a).

The present discussion will be limited to the origin of this unidirectional hysteresis found at low fields. This effect can be understood qualitatively very well if it is assumed that the film contains small regions with negative anisotropy, $-K_2$ is of the order of K_1, the anisotropy of the bulk of the film. The observations of Smith[21] indicated the existence of such regions, which have been suggested by him to account for films with $h_c \ll 1$.

---

*The composition of the films, measured generally about a 1000Å thick, varied between 77 and 83% Ni. This includes several films kindly provided by A. Noreika, Philco Corp., D. O. Smith, Lincoln Laboratory and M. Prutton, I. C. T.

**Uniaxial hysteresis is defined as two irreversible jumps of the magnetization, 180° apart in every 360° rotation of h. Unidirectional hysteresis is defined as one irreversible jump in every 360° rotation.
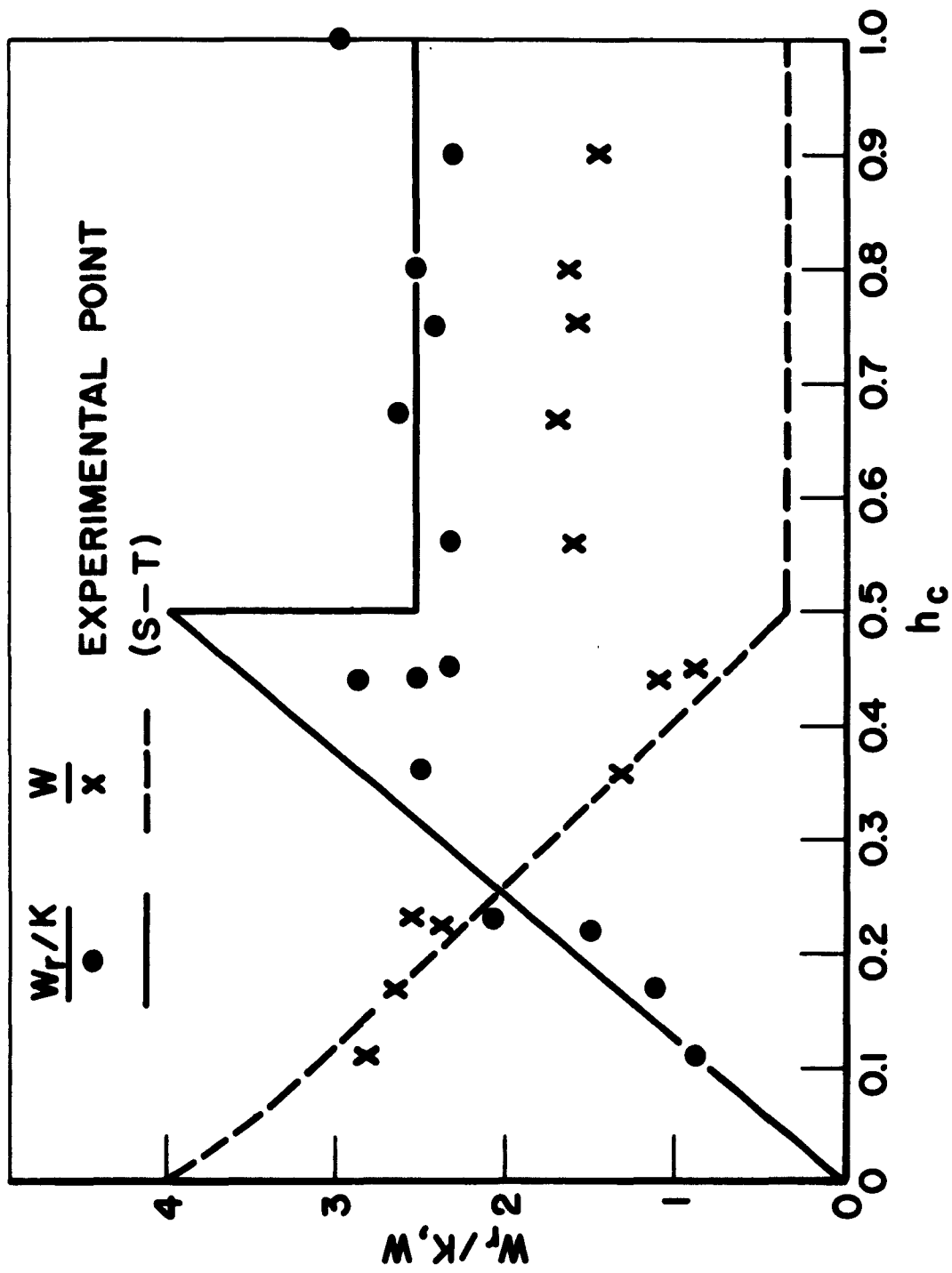
Fig. 19 - The dependence of the maximum reduced rotational hysteresis, W_r/K, and the rotational hysteresis integral, W, on the reduced coercive force h_c. The theoretical curves are derived from the Shtrikman and Treves (S-T) model which reduces to the Stoner and Wohlfarth (S-W) model for $h_c > 0.5$.
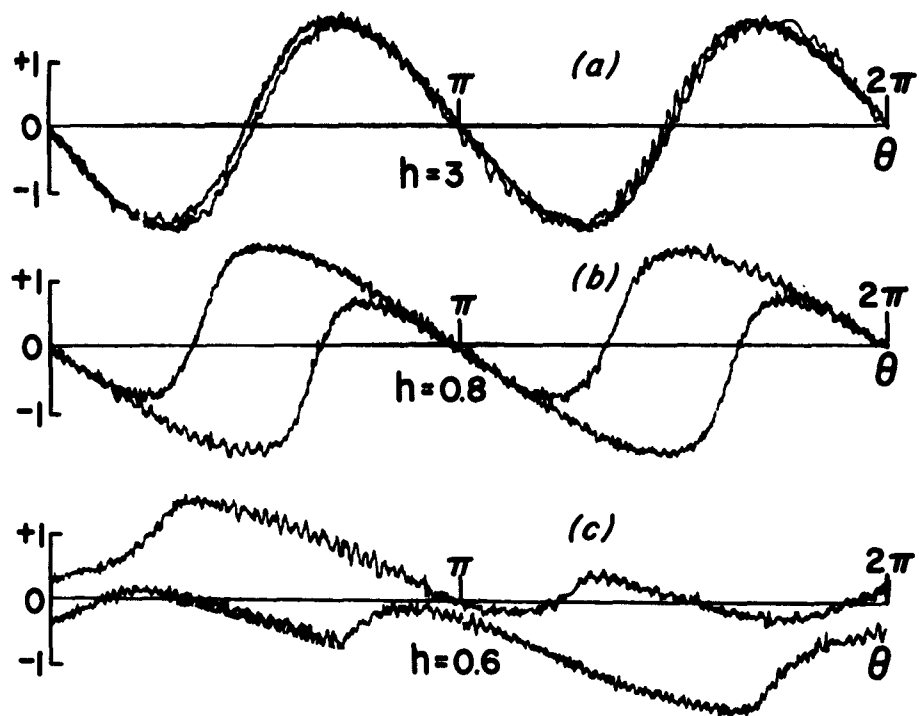
Fig. 20 - *Experimental torque curves for various values of the reduced applied field,*
h; (a) h = 3, (b) h = 0.8, (c) h = 0.6.
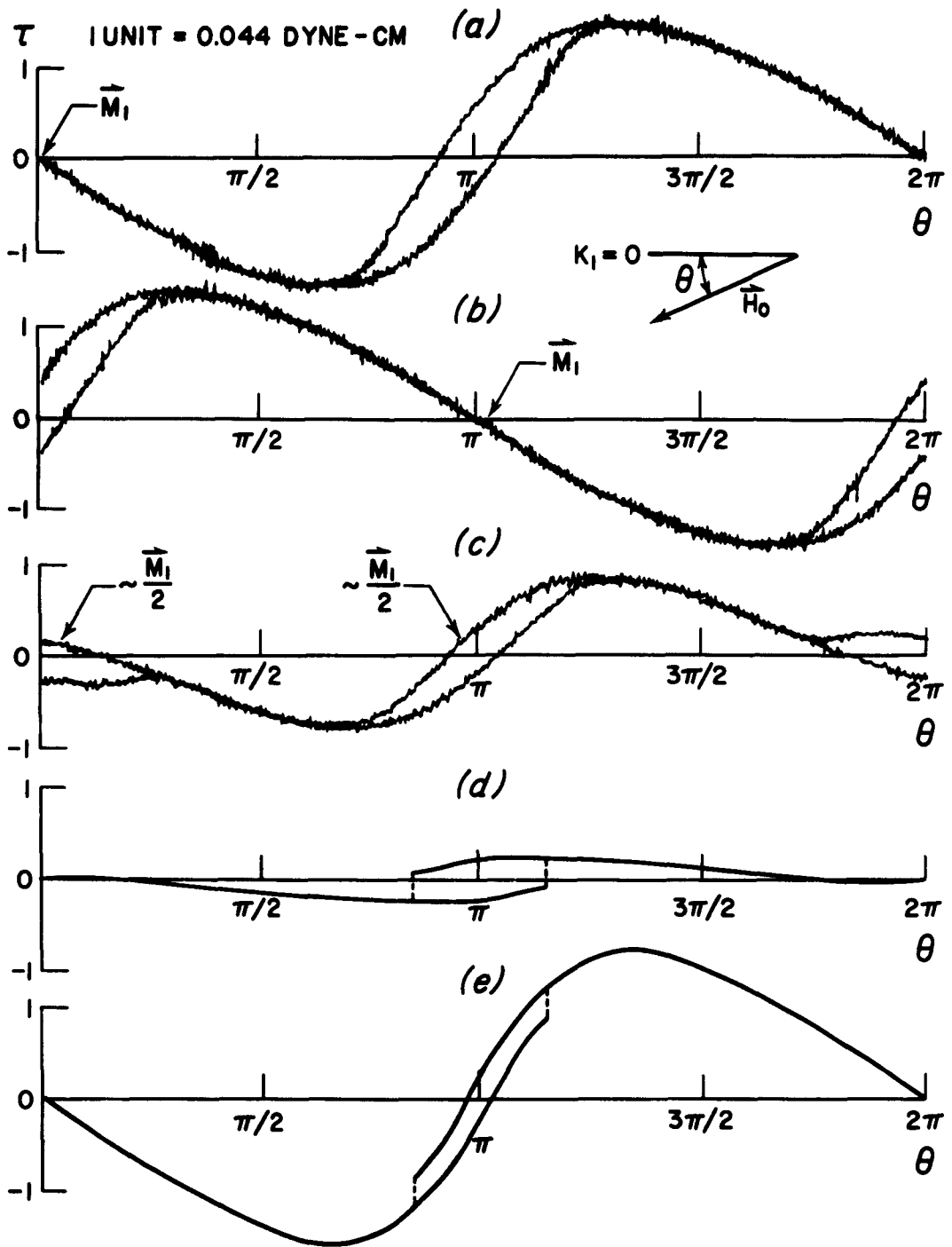
Fig. 21 - Experimental and theoretical torque curves; (a) shows the result if the film is first saturated in the $\theta = 0$ direction, (b) if the film is saturated in the $\theta = \pi$ direction, and (c) if the film is demagnetized. In each case, $h = 0.4$, and the torque is recorded for both clockwise and counterclockwise rotations. In (d), the torque calculated for an N. A. region is shown; (e) includes the interaction with M_1.

32

Consider a rotational hysteresis experiment in a negative anisotropy (N. A.) region described in terms of the (S-W) asteroid[22](Fig. 22). Let the easy axis of the bulk of the film be the y axis. Then, the x axis defines the easy axis of N. A. regions. If the total volume fraction of the N. A. region is small, the first-order effect of the bulk of the film, saturated in the + y direction, can be represented by an effective field $\vec{H}_{DC}$, also in the + y direction, along the hard axis of the N. A. region. Obviously $\left|\vec{H}_{DC}\right|$ is determined by the size and shape of the N. A. region. If the applied field $\vec{H}_o$, is then rotated by 360°, the circle it describes in the (H_x, H_y) plane will be shifted a distance $\left|\vec{H}_{DC}\right|$ towards the cusp in the + y direction and will not, as in the normal case, be symmetric with respect to the asteroid.*

Figure 21(d) shows the angular dependence of the torque $\vec{M}_2 \times \vec{H}_o$, where $\vec{M}_2$ is the magnetization of the N. A. region, for clockwise and counterclockwise rotation H_o, for the particular case $K_1 = 2K_2$, $\left|\vec{H}_o\right| = 0.4H_{k_1}$, and $\left|\vec{H}_{DC}\right| = 1.1H_{k_2}$. The calculation was made by determining $\vec{H}_e$, where $\vec{H}_e = \vec{H}_o + \vec{H}_{DC}$ for various orientations of $\vec{H}_o$. Then, using $\vec{H}_e$, the position of $\vec{M}_2$ was found from the tables provided by Stoner and Wohlfarth[15].

The general features of the curve can, however, be deduced by examining Fig. 22. As $\vec{H}_o$ is rotated clockwise, $\vec{M}_2$ will be moved reversibly, as long as $\vec{H}_o$ is in either the first, third, or fourth quadrants. In these areas, $\vec{H}_e$ either lies outside the asteroid or $\vec{H}_e$ and $\vec{M}_2$ already lie in the same quadrant. Only in the second quadrant, when $\vec{H}_o$ crosses the asteroid at A does an irreversible jump occur, the only one in a complete cycle of 360°. For counterclockwise rotations, $\vec{M}_2$ is moved reversibly when $\vec{H}_o$ is in any quadrant except the third. There, $\vec{M}_2$ jumps when $\vec{H}_o$ crosses the asteroid at B. Thus, in this picture, the only part of the torque which is irreversible occurs between the points A and B, straddling an easy direction of the bulk of the film.

If the torque, $\vec{M}_1 \times \vec{H}_o$, due to the interaction of $\vec{H}_o$ with the bulk of the film is superimposed, assuming that the volume fraction of the total N. A. regions is < 0.2, the result, Fig. 21(e), is seen to be qualitatively in agreement with experiment, Fig. 21(a).

According to the proposed model, the direction about which the loss occurs should be opposite to the direction of $\vec{H}_{DC}$, and, therefore, of $\vec{M}_1$. This has, in fact, been verified experimentally. Figure 7(a) shows the unidirectional loss occurring around $\theta = \pi$, after the film had been first saturated at $\theta = 0$. In Fig. 21(b), the loss shifted to $\theta = 0$, after the film was saturated at $\theta = \pi$. When the film was demagnetized by splitting it into domains, half the N. A. regions experienced an interaction field in the $\theta = 0$ direction, and half in the $\theta = \pi$ direction. The loss then appeared as expected, around both directions, Fig. 21(c).

---

*It is assumed that $H_o < 0.5H_{k_1}$, so that the bulk of the film behaves essentially as a permanent magnet.

33
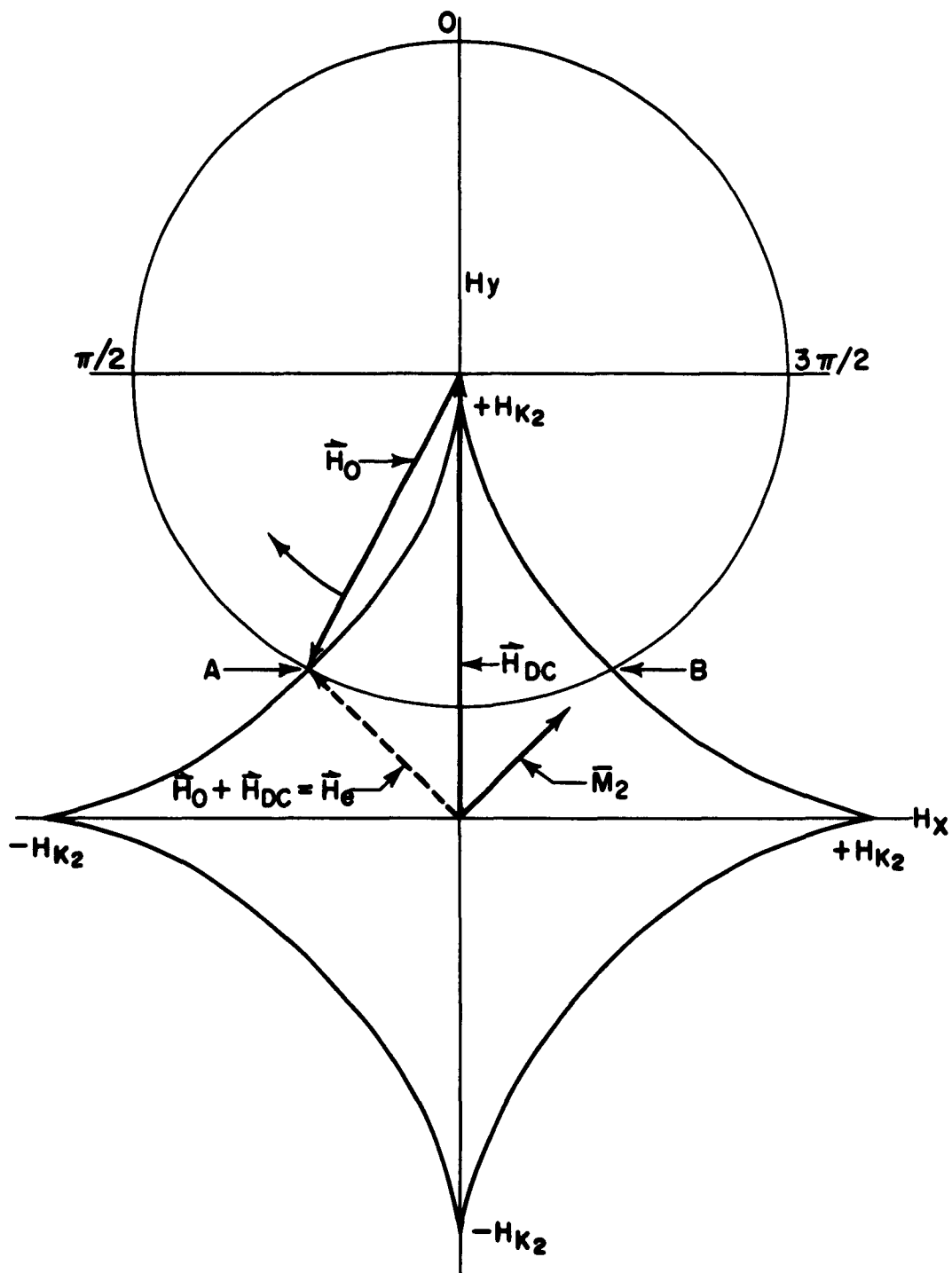
Fig. 22 - The (S-W) critical switching curve applied to an N. A. region. The effect of the bulk film saturated in the + y direction is represented by the field H_{DC}. The x axis defines the easy axis of the N. A. region.

The magnitude of the unidirectional loss (observed in a series of films whose h_c varied from 0.4 to 1.5) has been found to increase sharply above $h_c = 0.7$. This is indicative of a similar increase in the total volume fraction of N. A. regions, in agreement with Smith's[21] results.

It is concluded that the field dependence of the rotational hysteresis becomes quite complex when h_c is not $\ll 1$. The unidirectional hysteresis observed at low fields in films with $h_c > 0.5$ can be understood qualitatively if the existence of regions with negative anisotropy is assumed. Results interpreted in terms of this model indicate that the total volume fraction of negative anisotropy regions increases sharply above $h_c = 0.7$. An analytic treatment of the model, which will allow a quantitative interpretation of the experimental data, is presently being considered.

3) The Nature of Unidirectional Hysteresis

A series of experiments in which the effect on the unidirectional hysteresis of a steady field, $\vec{H}_a$, applied parallel to $\vec{M}_1$ (and hence $\vec{H}_{DC}$), was in progress at the close of the contract. The object of these experiments has been to try to put quantitative values on the magnitudes of the interaction field, $\vec{H}_{DC}$, and the anisotropy, H_{k_2}, and to suggest a model for -K regions. The following preliminary results were obtained.

(i)   Unidirectional loss occurs in films with $h_c > 0.5$.

(ii) The unidirectional loss always occurs for $h_0 > 0.5$.

(iii) The unidirectional loss is always accompanied by a uniaxial loss at fields $H_0 > H_{k_1}$.

(iv) The unidirectional loss shifts 180° when M_1 is reversed.

(v)   The unidirectional loss increases for increasing H_a antiparallel to M_1 and decreases for increasing H_a parallel to M_1.

(vi) If H_0 and H_a are changed together, so as to maintain $(H_0 - H_a)$ constant, the unidirectional loss is not constant. In fact, it is larger for small positive or negative values of H_a than for $H_a = 0$ but decreases when H_a becomes large.

(vii) If H_a is applied along the hard direction of the main film, then the unidirectional loss is constant for $h_a = 0$ and $h_a = \pm 0.2$.

The following suggestions are made as a consequence of these results:

(i)   There is a distribution of easy directions in the small "K" regions. (Result (vii))

(ii) H_{DC} is a function of H_a. (Result (vi))

(iii) The asteroid model (Fig. 22) is only qualitatively correct. (Results (iv) and (v))

35

Two models for "-K" regions have been invented and are being investigated:

(a) <u>Antiferromagnetic inclusions</u> The anisotropy of antiferromagnetic oxides, like NiO, is such that its spins line up normal to an applied field. Thus, inclusions of NiO in a ferromagnetic matrix will have their spins normal to the magnetization of the matrix. Exchange coupling can therefore result in there being a ferromagnetic region immediately around the NiO inclusions, having their easy axes normal to that of the main film.

(i) <u>Anisotropy of the regions</u>

For a ferromagnetic region of volume V around an antiferromagnetic inclusion of volume v and anisotropy K_a, the anisotropy will be of the order of $K_a v/V$. K_a for NiO is of the order of 10^5 ergs/cc so v/V of the order 10^{-2} gives anisotropies of the order of those found in the films.

(ii) <u>Scale of the regions</u>

The magnetization distribution is similar to that in a Néel wall so we may anticipate the -K regions to be of the order of 2-10 μ wide. This is the case.

(iii) <u>Density of regions</u>

The data of Uhlig et al[23] leads to the expectation that, at 400 °C, there will be 0.5μ gm/cm^2 of oxygen in a film of mass 80μ gm/cm^2. This is consistent with a concentration of 10^5 NiO regions of radius 1,000 Å per sq. cm. of film. This is of the observed order of magnitude.

(b) <u>Elongated regions</u>

A similar model has recently been independently proposed by Thomas[24] Here the -K regions are regarded as arising from regions with the same easy direction of induced anisotropy as the matrix, but with a different anisotropy magnitude, H_{k_2}. Further, these regions are elongated normal to the easy direction.

Simple analysis of these regions shows that:

$$H_{DC} = H_{k_e} + H_{k_2}, \text{ where the effective anisotropy of the regions is } H_{k_e}$$

From result (ii), and the asteroid model, it can be seen that, for this model of -K to apply, the regions must have $H_{k_2} \sim 0.5 H_{k_1}$

Neither model explains the results entirely and further investigation is required.

B) Determination of the Anisotropy in Thin Permalloy Films

The induced uniaxial anisotropy in thin Permalloy films is generally assumed after Smith [25] and Olson and Pohm [26] to be of the form

$$E_k = K \sin^2\theta \tag{7}$$

Here, E_k is the anisotropy energy per unit volume, K is the anisotropy constant, and θ is the angle between the saturation magnetization I_s and the easy axis ($E_k = 0$). Experimentally, what is normally measured is not K but the saturation field in the hard direction H_k, and it is assumed[27] that

$$H_k = \frac{2K}{I_s} \tag{8}$$

When Eq. 8 was first considered applicable to films, it was believed that the magnetization processes in a thin film were coherent and essentially the same as those in a single-domain particle with a unique uniaxial anisotropy[15]. For that model, a linear reversible hysteresis loop is expected in the hard direction with $H_k = 2K/I_s$. However, it is now known[28-30] that the coherent-rotation theory applied to films is very often inadequate. Although the discrepancies between the theory and the observed behavior appear to decrease in proportion to the angle between the applied field and the hard axis, it nevertheless seems appropriate to investigate experimentally the relationship between H_k and K.

In this paper, the results of four independent types of measurements, all yielding H_k on the basis of the coherent model, are compared: (A) hysteresis loop; (B) high field torque; (C) rotational hysteresis; (D) torque 90° to the easy axis. In the cases where discrepancies are found, it is shown that they are attributable to a dispersion in both the direction and magnitude of the anisotropy. Finally, a torque method to determine this dispersion is discussed.

DETERMINATION OF H_k

A value of field, equal to H_k in the coherent model, was obtained from each of the four types of measurement described in the following.

(A) Hysteresis loop: Using a low-frequency loop tracer[31], a value for H_k can be determined from the hysteresis loop observed in the hard direction. Unfortunately in most instances, as the applied field approaches the saturation field, the loop becomes irreversible and the exact saturation point is difficult to determine. The generally accepted method[25,26] is to reduce the field below the onset of hysteresis and then to extrapolate the linear portion to the saturation level, calling the field at the intersection point H_k.

(B) High field torque: Recently, with the development of sensitive torque magnetometers, it has become possible to measure the angular dependence of the torque in thin films as a function of applied field[30,32-34]. For applied fields $H \gg H_k$, the torque τ may be defined[35] as

$$\tau = -V \frac{dE_k}{d\theta} \tag{9}$$

37

where V is the volume of magnetic material present. Substituting E_k from Eq. 7,

$$\tau = -KV \sin 2\theta \tag{10}$$

Measurement of the volume and maximum amplitude ($\tau_{max} = KV$) of the high field torque (Fig. 23) allows K to be determined directly from Eq. (10). Actually, it has been found[30] in Permalloy films that τ_{max} becomes field-independent for $H > H_k$, so that the use of extremely high fields seems unnecessary.

Rather than attempt to determine the volume, the saturation moment, $\mu_s = I_s V$, was measured directly in a moment balance[36]. Then, from Eq. (8), a value for H_k was calculated, from $\tau_{max}/\mu_s = K/I_s$.

(C) Rotational hysteresis: In the coherent model, the rotational hysteresis per unit volume W_r is zero for applied field $H > H_k$[37]. This means that the field at which W_r goes to zero should also be H_k. The angular dependence of the torque was recorded for 360° clockwise and counterclockwise rotations of H. Since $W_r = \int_0^{360} L d\alpha$, where L is the torque per unit volume and α is the angle between $\overline{H}$ and some fixed direction, the field at which the area defined by the two torque curves went to zero was considered to be H_k.

(D) Torque 90° to the easy axis: The torque as a function of field, 90° to the easy axis of a single-domain particle with uniaxial anisotropy, can be calculated readily[38,39] assuming the coherent model. The result, plotted in Fig. 24, is

$$\tau = H \mu_s \left[1 - \left(\frac{H}{H_k}\right)^2 \right]^{1/2} \tag{11}$$

This function has several interesting properties. From Eq. 11, $\tau = 0$ when $H = H_k$. Also, the maximum torque given by $d\tau/dH = 0$ occurs at $(1/\sqrt{2})H_k$, and its amplitude at this point is $0.5 H_k \mu_s$.

The film was saturated in the easy direction and the torque recorded as a function of increasing field in the hard direction. The hard direction was taken as that direction in which, for a field $\gg H_k$ decreasing to zero, the torque was zero. The field at which the maximum in the torque occurred was taken as $(1/\sqrt{2})H_k$.

EXPERIMENTAL RESULTS

Values for H_k for several Permalloy films have been determined from the four techniques described in the foregoing, and the results are summarized in Table II. All the films were in the composition range 77-83% Ni and were prepared by evaporation*[40], except No. 8 which was sputtered**.

*Films No. 5,6,7, and 9 were kindly provided by D. O. Smith, Lincoln Laboratory, MIT, Lexington, Massachusetts.

**Film No. 8 was kindly provided by A. J. Noreika, Philco Corporation, Blue Bell, Pennsylvania. See M. H. Francombe and A. J. Noreika, J. Appl. Phys. 32, 97S (1961).
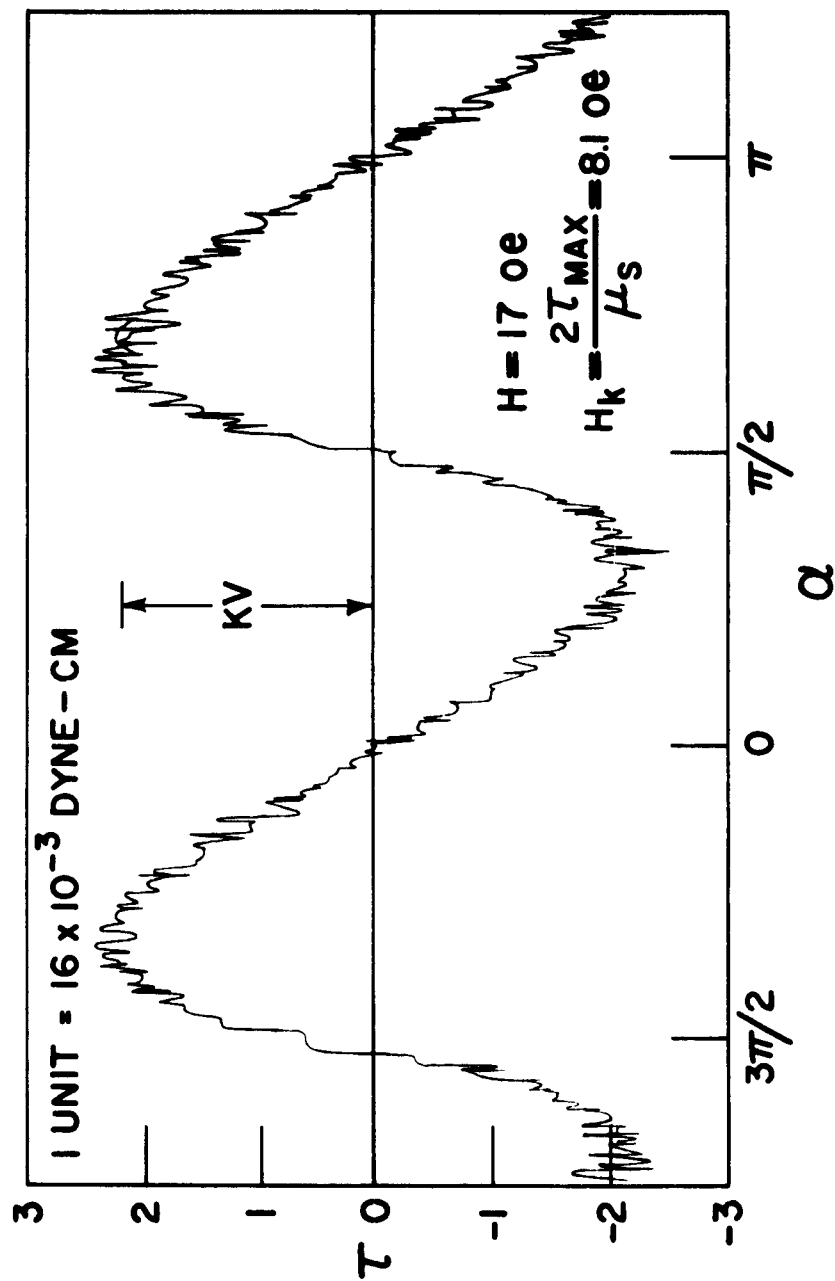
38

Fig. 23 - Angular dependence of the high field (H= 17 oe) torque in film No. 1.
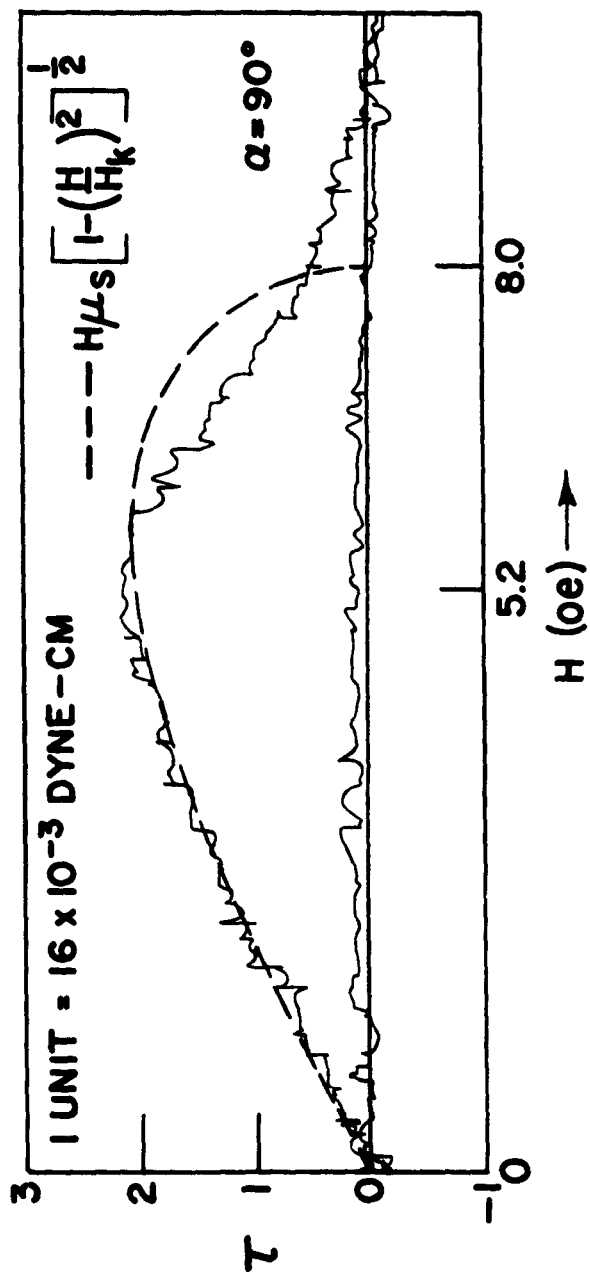
39

Fig. 24 - The torque vs. applied field, 90° to the easy axis of film No. 1, after saturation in the easy direction. The theoretical curve was calculated for $H_K = 8.0$ oe.

Comparison of columns A and B in Table II shows that the values of H_k determined from the hysteresis loops and the high field torques agree reasonably well. In film No. 9 where the largest discrepancy exists, the hysteresis loop in the hard direction was linear only for $H < 0.2\ H_k$, necessitating a long extrapolation to saturation. In all the other films the hysteresis loops in the hard direction was linear and reversible, at least up to $H = 0.5\ H_k$. Using this as an arbitrary limit, it is concluded that, if the hysteresis loop in the hard direction is linear and reversible up to $H = 0.5\ H_k$, the value of H_k obtained by extrapolation to saturation will be equivalent to $2K/I_s$, where K is determined from the amplitude of the torque at high fields.

The values of H_k determined from the rotational-hysteresis method are listed in column C. Obviously, a large discrepancy exists between these results and those shown in columns A, B, and D, especially when $H_c/H_k > 0.4$. Here, H_c is the coercive force in the easy direction. This is not unexpected, since it has been shown[32,41,42] that the rotational hysteresis in films very often does not go to zero but maintains a constant value even at fields as high as 700 oe. The persistence of hysteresis at fields in excess of the H_k values found from the hysteresis loops can be interpreted as a distribution in the magnitude of the anisotropy. Assume that most of the film has a single $H_k = H_k'$. Let the remainder of the film also have a single $H_k = H_k''$, where $H_k'' > H_k'$. In both the hysteresis loop and the high field torque, if the amount of material with H_k'' is $< 5\%$ of the total, its presence would be difficult to detect and the measured H_k would be very nearly H_k'. If the rotational hysteresis is now determined as a function of applied field, the loss will not go to zero at H_k', but will persist until H_k''. Thus, the rotational-hysteresis experiment detects only the effect of material whose H_k is larger than the measuring field. In the case of a magnitude distribution in the anisotropy, this appears as a high field tail on the experimental curve.

The values of H_k deduced from the 90° torque are listed in column D. While the results agree fairly well with those shown in columns A and B, they are, on the average, slightly lower. Figure 24 shows a typical experimental 90° torque curve recorded for film No. 1 and compared to the theoretical curve (Eq. 11) for $H_k = 8$ oe. The failure of the torque to go to zero near 8 oe confirms the rotational-hysteresis data and shows that material with an $H_k > 9$ oe must be present in film No. 1. It is to be noted, however, that similar curves have been calculated by Flanders[43], assuming an angular dispersion only in the anisotropy directions of an assembly of single-domain particles. Since an angular dispersion is known[44] to exist in Permalloy films it is concluded that a dispersion in both the magnitude and direction of the anisotropy exists in Permalloy films. This is supported by the following experimental evidence.

Table II

THE VALUES OF H_k DETERMINED FOR SEVERAL PERMALLOY
FILMS FROM A) HYSTERESIS LOOP, B) HIGH FIELD TORQUE,
C) ROTATIONAL HYSTERESIS, D) 90° TORQUE.

FILM NO.	$\frac{H_c}{H_k}$	t (Å)	H_k (oe)			
			A	B	C	D
1	0.12	1400	8.0	8.1	10.0	7.3
2	0.17	1500	5.8	6.2	7.1	5.7
3	0.22	1500	4.6	4.9	5.0	5.1
4	0.36	1000	4.0	3.4	10.2	3.3
5	0.45	500	4.2	3.7	>100	4.0
6	0.64	800	3.1	3.1	>100	2.8
7	0.90	750	3.2	3.6	>100	3.0
8	1.0	1000	3.4	3.1	>100	3.2
9	1.7	600	3.7	2.9	>100	3.2

A = HYSTERESIS LOOP

B = HIGH FIELD TORQUE

C = ROTATIONAL HYSTERESIS

D = 90° TORQUE

DISPERSION IN THE ANISOTROPY

Dispersion in the anisotropy of thin films has been discussed both theoretically[45,46] and experimentally[44,47]. In the methods which have been described to measure dispersion, it was assumed that the dispersion existed only in the direction of the anisotropy and that the interaction between regions with different orientation could be neglected.

Recently, Flanders and Shtrikman[48] have developed a torque technique for determining the anisotropy distribution in single-domain powders. Its extension to films has been carried out and is discussed for the particular case of film No. 1.

The extension is based on the following assumptions:

(1) The interactions between regions in the films with different anisotropy directions and magnitudes can be neglected. This means that only an effective distribution is found which, since the nature of the interaction is unknown, may be dependent on the experimental method employed.

(2) If one considers only the material in the film which has the same anisotropy magnitude and direction, the torque response of that material in the saturated condition to a field 90° to its easy axis will be given by Eq. 11, as the field is initially increased from zero. However, as the field is then reduced to zero from some value greater than H_k, the torque will be zero, since the magnetization of the material will split by the formation of domains, such as to give two equal but opposite components along the easy axis.

The procedure is as follows: The film is saturated in the easy direction as determined from the high field torque. The field is then applied at some angle ϕ less than 90° from the easy direction, increased from zero to some value higher than the highest H_k in the film, and then reduced to zero. If the torque is reversible, then the angular dispersion is less than $(90 - \phi)$. ϕ is increased and the cycle repeated until at $\phi = \phi_c$, the torque becomes irreversible. The angular dispersion δ is then defined as $\delta = \pm (90 - \phi_c)$. Figure 25 shows the result for film No. 1 in which $\delta = \pm 7°$.

The next step involves subtracting the decreasing field torque from the increasing field torque at each angle to separate the 90° torque contribution of each sector. This has been done for film No. 1, and the reduced torque curves so obtained are plotted in Fig. 26. If the distribution in magnitude of the anisotropy in each sector is not too different (which is indicated for film No. 1 by the similarity between the curves), the volume fraction, v, in each sector is proportional to the amplitude.

To determine the dispersion in the magnitude of the anisotropy, the entire procedure is essentially repeated. However, instead of increasing the field continuously at each angle to a value higher than the highest H_k it is increased in steps in the following manner. The field is cycled from zero to a field H_1 and back to zero. Here, H_1 is lower than the lowest H_k in the sector. The field is
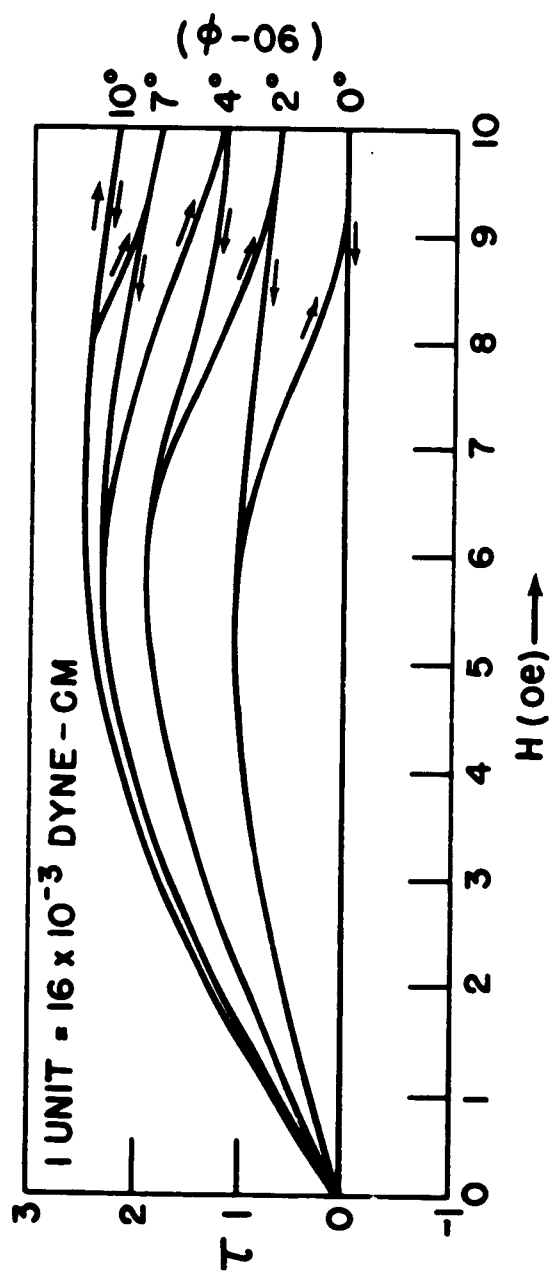
Fig. 25 - The torque vs. applied field as a function of the angle (90-φ) which the field makes with the hard axis. The curves shown were redrawn from the recorded ones which were obtained by cycling the field as indicated by the arrows. The film was initially saturated in the easy direction.

44
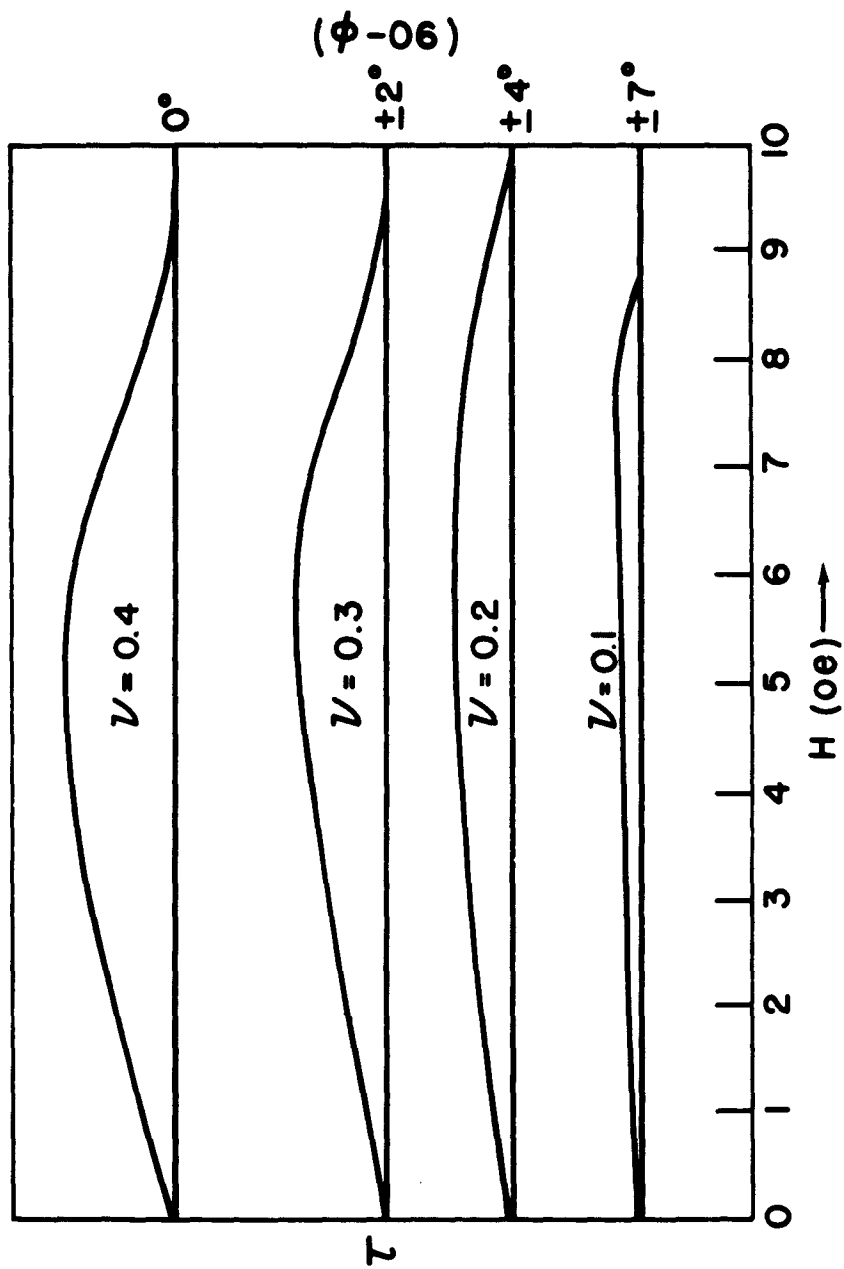
Fig. 26 - Reduced-torque curves for film No. 1 obtained from the curves shown in Fig. 3 by subtracting the torque for decreasing field from the torque for increasing field at each value of $(90-\phi)$. The volume fraction, v, for each sector was found by assuming the torque amplitude to be proportional to the volume of material in that sector.

45

increased to H_2 where $H_2 > H_1$ and reduced again to zero. If the torque is irreversible, all the material associated with the decrease in torque is assigned an average H_k, $\langle H_k \rangle = (H_1 + H_2)/2$. This process is repeated until the torque again becomes reversible at a field H_n where H_n is higher than the highest H_k in the sector.

The reduced torque curves for film No. 1 are shown in Fig. 27. The signal-to-noise ratio was too low at $\pm 7°$ for any meaningful determination of the distribution in magnitude. The volume fraction, v, contributing to each curve was taken to be proportional to $A/\langle H_k \rangle^2$, where A is the area of each curve and $\langle H_k \rangle$ is the average H_k assigned to it. The final total distribution is shown in Table III.

The fact that the increments in ϕ and H were taken relatively large leads to an appreciable error. For example, all the material whose easy axis lies between 2° and 4° away from the average easy axis was treated as if it were concentrated at 2°. This weights the lower $\langle H_k \rangle$ brackets too heavily since, in the model used, an applied field at 92° to the easy axis of some material reverses the magnetization of that material at h = 0.96 and not at h = 1 as assumed. While this error could be made superficially negligible by taking very small increments both in angle and field, the crudeness of the assumed model does not justify extending the procedure to such fine details.

<div align="center">CONCLUSIONS</div>

It is concluded that if the hysteresis loop of a thin Permalloy film in the hard direction is linear for $H > 0.5H_k$, the value of H_k obtained by extrapolation to saturation will be equivalent to $2K/I_s$, where K is determined from the amplitude of the torque at high fields. The values of H_k determined as described from rotational hysteresis and 90° torque curves are too high and too low, respectively, because of a dispersion in both the magnitude and direction of the anisotropy. Using a torque method, it is possible to determine experimentally the effective dispersion.

C) Oblique Incidence Anisotropy

The formation of a special anisotropy in thin films due to evaporation at an angle to the film normal has been discussed by several authors[2,49,50,51]. Knorr and Hoffman[50] originally proposed that the formation of a texture axis was responsible for the effect, but this was shown to be incorrect by Pugh et al[51]. Various experiments, generally in very thin films (200Å), by Smith et al[2] led them to propose a geometric self shadowing model which caused the formation of anisotropy chains perpendicular to the beam. Recently, a more complicated situation at grazing incidence has been found by Cohen[52], and a model based on the elongation of chains parallel to the incident beam was suggested.

With the exception of the data of Pugh et al, the value of the anisotropy has always been inferred from the measurement of the slope of the hysteresis loop in the hard direction. For the very large anisotropy values often encountered ($H_k = 30 - 3000$ oe), this is a very doubtful technique since the maximum fields available are relatively small. For this reason, it was felt that a determination
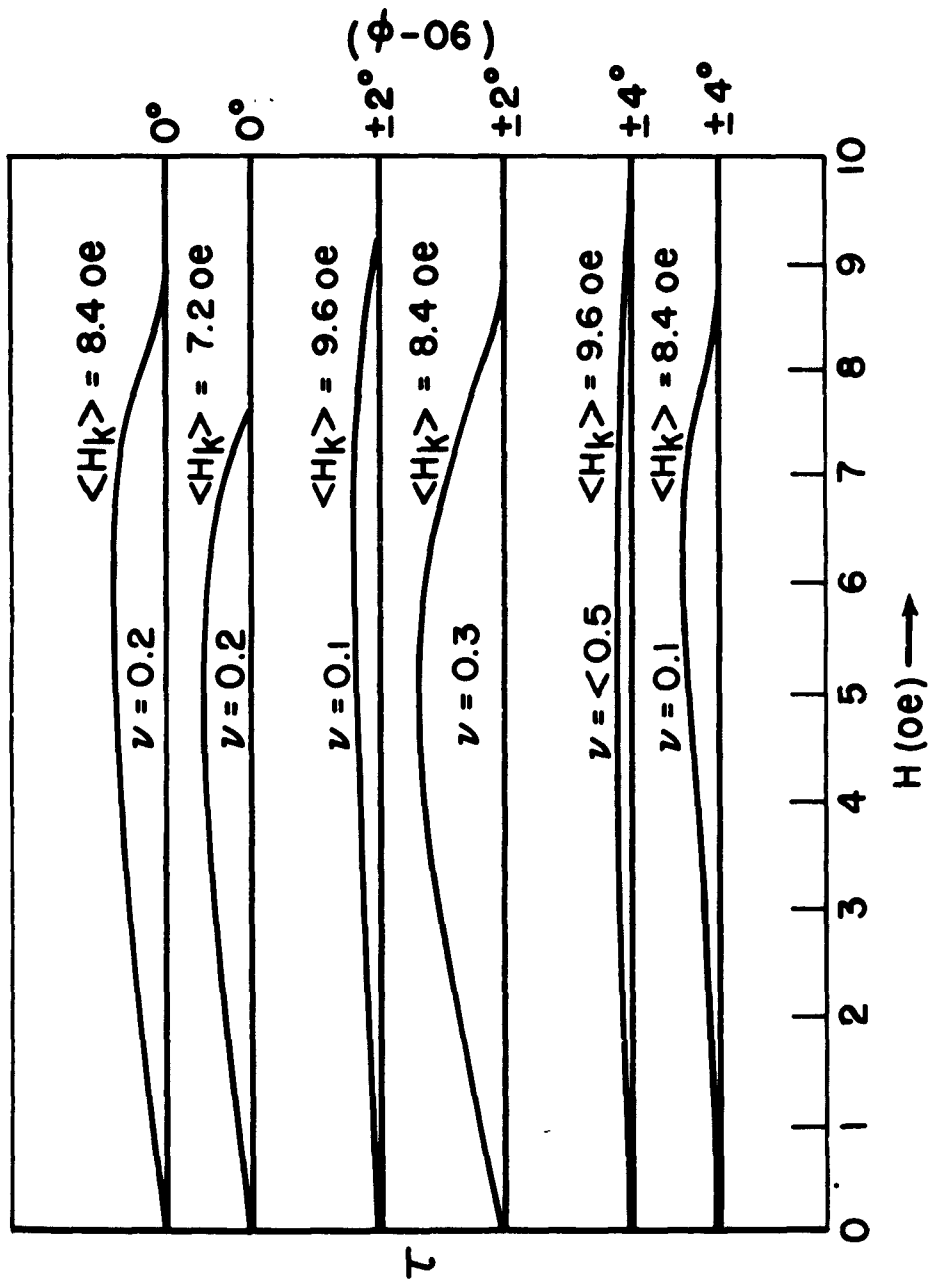
Fig. 27 - Reduced-torque curves for film No. 1, considering the dispersion in both the magnitude and direction of the anisotropy. The volume fraction ν assigned to each curve was found by assuming each curve represented a volume proportional to $A/\langle H_K \rangle^2$, where A is the area of the curve and H_K is the average H_K assigned to it. At $(90-\phi) = \pm 7°$, ν was taken to be 0.1.

47

Table III

EFFECTIVE DISPERSION IN THE MAGNITUDE AND DIRECTION OF THE ANISOTROPY FOR
FILM #1, SPECIFIED IN TERMS OF THE VOLUME FRACTION ν

$(\phi - \phi_0)$	$\langle H_k \rangle$			TOTAL VOLUME FRACTION
	9.6 oe	8.4 oe	7.2 oe	
0°		0.2	0.2	0.4
±2°	0.1	0.3		0.4
±4°	<0.05	0.1		~0.15
±7°	< 0.1			~0.05

of the anisotropy directly, by torque measurements, as a function of incident angle was a worthwhile experiment. Later, with the development of a vibrating sample magnetometer, the entire hysteresis loop could be plotted, and very often this was used to determine the anisotropy.

The intent to measure high anisotropy films lead to the consideration of the spurious torque which will arise if the film is not exactly in the plane of the rotating field.

Consider a film, originally in the x-y plane, rotated about the x-axis by an angle θ_0 (Fig. 28). Let the applied field H_0 lie in the x-y plane at an angle ϕ to the x-axis. Let the easy axis of anisotropy, K, be at an angle α to the x axis. Then $\vec{M}$, the saturation magnetization, can be described by the polar coordinates ϕ and θ. The angle between $\vec{M}$ and the film is β, and the projection of M on the film and the x-axis is ψ. Since, experimentally, the z-axis coincides with the magneto-meter suspension axis, one wishes to determine $|\tau_z|$, the magnitude of the torque per unit volume in the z direction. This is done by determining the equilibrium position of $\vec{M}$ for a given set of values of θ_0, K, α, H_0 and ϕ_1.

To obtain an order of magnitude value, consider an isotropic film, i.e., K = 0. Then the calculation is straightforward since only two torques are involved, one due to the demagnetizing field and one due to the external field. For equilibrium, they must be equal and opposite, i.e., M, H_0 and n, the unit normal to the films must lie in the same plane. In this case

$$|\tau| = -\frac{M^2 N}{2} \sin 2\beta + MH_0 \sin (\gamma - \beta) \tag{12}$$

where N is the demagnetizing coefficient perpendicular to the plane of the film, $(\gamma - \beta)$ is the angle between $\vec{M}$ and $\vec{H}_0$, and γ is given by

$$\sin \gamma = \sin \theta_0 \sin \phi_1 \tag{13}$$

Setting Equation (12) equal to zero, one gets the equilibrium condition

$$\frac{MN}{2} \sin 2\beta = H_0 \sin (\gamma - \beta) \tag{14}$$

The torque per unit volume measured is the reaction, in the z direction given by

$$|\tau_z| = \frac{\sin \theta_0 \cos \phi_1}{\cos \gamma} \left[MH_0 \sin (\gamma - \beta) \right] \tag{15}$$

Using $2\pi M = 5 \times 10^3$ emu/cc., the value for Permalloy, and $\phi_1 = 50°$, various values θ_0 and β were substituted in Equation (14), and H_0 was calculated. These values were then substituted into Equation (15) and $|\tau_z|$ was determined.
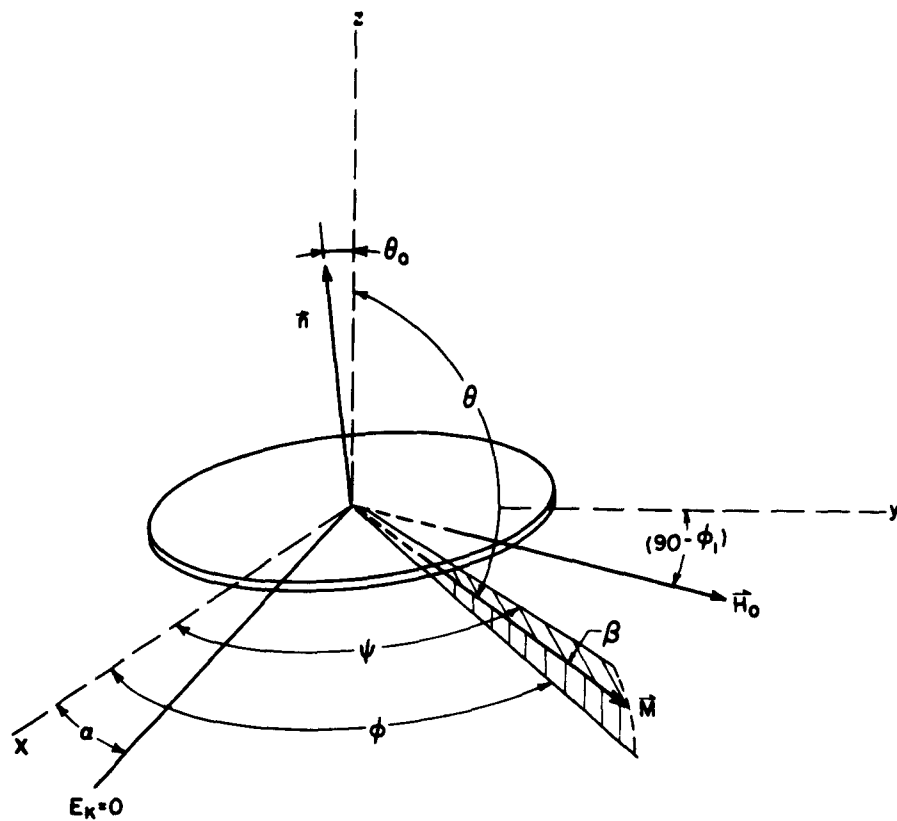
Fig. 28 - Film tilted away from the plane of the rotating field.

Table IV

TORQUE PER UNIT VOLUME IN A TILTED ISOTROPIC PERMALLOY FILM

$\phi_1 = 50°$	θ_o	H_o(oe)	$\left|\frac{T}{s}\right|$ erg/cc
	1°	165	$.013 \times 10^3$
		1260	.13
	5°	75	.22
		1460	3.8
		10,800	16
	10°	110	1.4
		1470	15
		6420	47

Table IV is a summary of several typical values. They are in good agreement with the recent work of Schuppel et al[55], who have carried out a similar calculation. These results show that if the anisotropy field H_k is given by $\frac{2K}{I_s}$, which will be true for low dispersion films, the error introduced by a 5° tilt is $< 10\%$ for measuring fields $< 10H_k$.

The films were evaporated onto cold glass substrates held in the holder shown in Fig. 29. The distance from the crucible to the holder was carefully measured, and the angles to the various substrates were measured graphically. Figure 30 shows the value of the anisotropy constant as a function of the angle of incidence for both iron and Permalloy. The results for Permalloy are in good agreement with those obtained by Smith et al[2], Cohen[52] and Kambersky[54], including a 90° change in the easy direction for angles $> 70°$. A comparison of the magnetic thickness, i.e., the thickness determined from magnetic moment measurements assuming a value of I_s, and the optical thickness as determined by multiple beam interferometry on several Permalloy films is shown in Table V. The large discrepancies found, especially near 55°, in contrast to normal incidence films, indicate a large porosity which would be expected if the origin of the anisotropy was a net shape effect in an agglomeration of particles, Fig. (9). A similar effect has been observed by Kambersky[54].

The results for Fe, while qualitatively in agreement with those for Permalloy, show a considerable quantitative difference. From the data in Fig. 30 and in Cohen's[52] work, K for Fe generally seems to be about 3 times larger than that for Permalloy for the same angle. This is very probably associated with the difference in I_s for the two materials. Since shape anisotropy is proportional to I_s^2, K for Fe should be ~ 4 times that for Permalloy. If the particles interact, which they undoubtedly do, a factor of 3 is quite reasonable.

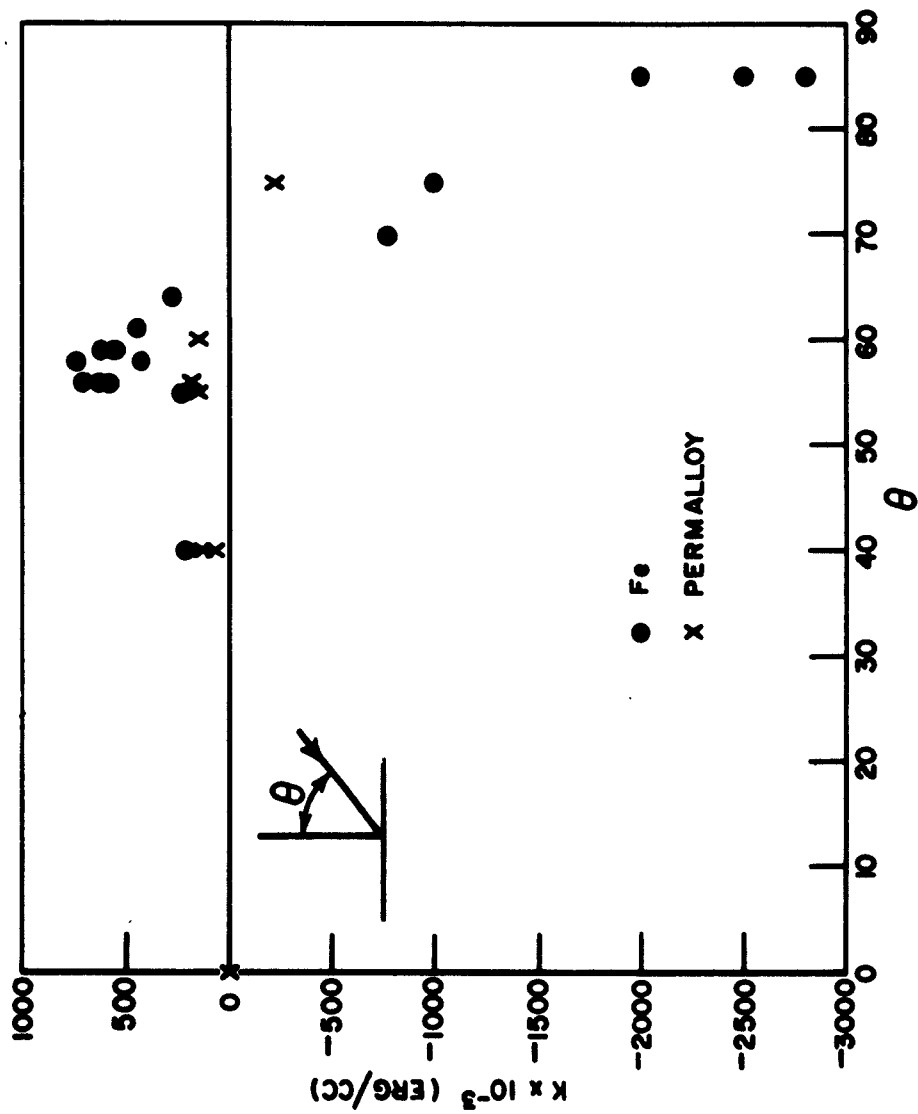Figure 29 - Photograph of sample holder for oblique incidence films.

52

Fig. 30 - The anisotropy as a function of the angle of incidence for both iron and Permalloy films.

Table V

OPTICAL THICKNESS VS MAGNETIC THICKNESS OF PERMALLOY FILMS

Angle of incidence (dg)	Optical thickness (Å)	Magnetic thickness (Å)
60	250	200
55	600	300
55	700	260
40	200	40
40	850	520
0	1500	1350

The reason for the extremely large anisotropy found at grazing incidence is clearly seen in Fig. (9). It appears that a very rough platelet structure is formed, strongly orientated towards the beam direction. This structural evidence was well corroborated in several films of this type, in which it was found that the easy axis could be as much as 20° away from the film plane.

It is therefore concluded that the anisotropy found at grazing incidence is caused by the elongated shape of individual particles formed during evaporation.

D) Film Grown Epitaxially

Several Permalloy (83% Ni) films which were grown epitaxially and deemed to be single crystals by electron diffraction studies, were examined in the torque magnetometer. In a few cases, no Sin 4θ component which would characterize the crystalline anisotropy could be found. In others, however, such a component was definitely observed in addition to the usual Sin 2θ uniaxial torque. Figure 31 shows the experimental torque curve for one of those films. These facts indicate that a certain minimum grain size is necessary to cause an observable crystalline anisotropy. That is, while the grain size in some sample may be large enough to give the diffraction pattern of a single crystal, it is apparently not large enough to exhibit crystalline anisotropy. It is felt that this is a very significant point and is one which was being pursued vigorously at the close of the contract.

E) Vibrating Sample Magnetometer

The study of the hysteretic properties of thin magnetic films has been hampered by the experimental limitations of the instruments used to determine this behavior. Until very recently, the only data available was that which could be derived from the a.c. hysteresis loops of films observed in instruments similar to that described by Crittenden et al[31] in 1951. Using the a.c. field technique, difficulties in reproducing the true shape of the hysteresis loop are often encountered[55]. Maximum field limitations are also imposed, since a.c. air-core coils rather than d.c. electromagnets provide the driving fields.

With the development of torque magnetometers for thin films[20,30,33,34] an important advance was made, particularly in the study of the nature of the anisotropy found in magnetic films. However, considerable care must be taken in the construction if the necessary sensitivity of 10^{-3} dyne-cm. is to be realized.
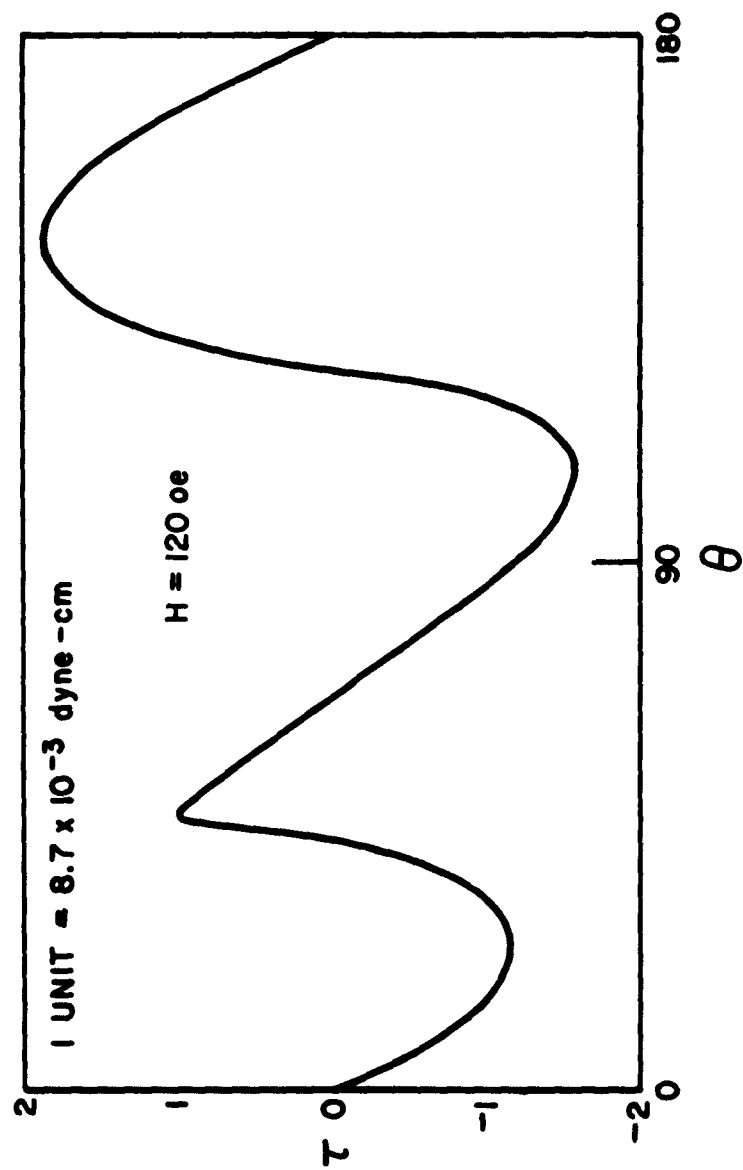
54

Fig. 31 - Torque curve on epitaxially grown Permalloy film.

Using a vibrating sample magnetometer[56-58], d.c. magnetic measurements have been made on thin films at this laboratory, from which it is possible to obtain all the information derived from both the loop tracer and the torque magnetometer. In this instrument, Figure 32, as in Foner's instrument[58], the sample is vibrated at 90 cps. normal to an applied d.c. magnetic field. The frequency and motion are provided by an 1800 rpm synchronous motor, a 1 to 3 gear ratio to achieve 90 cps., and an eccentric to transform the motion from rotational to reciprocal. The use of a motor drive provides a constant amplitude of sample motion. This is a particular problem with systems using loudspeaker drives, which become mechanically overloaded when large magnetic moment samples are measured at high fields requiring electronic feedback or null type measurements. A motor drive can also provide a large amplitude of sample motion and can accommodate heavy samples. Provision is made to adjust the amplitude of the vibration from .5mm to 4mm. The state of magnetization of the sample is sensed by a 2×10^4 cm^2 - turn coil which can be situated sufficiently far from the sample (~1 cm) to accommodate temperature control apparatus. The axes of the pickup coil and of the sample motion are parallel[58]. An identical coil for minimizing stray field changes is connected in series opposition with the pick-up coil and is located directly below it. After the 90 cycle sample signal is amplified, it is rectified by means of a phase sensitive detector using a 90 cycle reference signal and applied to a Mosley x-y recorder. As viewed on the recorder, a sensitivity of 5×10^{-5} emu has been obtained in measuring fields up to 10,000 oe. It has been found that the smoothness with which the applied field is changed is of extreme importance. The apparent noise level of the instrument can be varied by several orders of magnitude depending on the nature of the field power supply, as sudden changes in the field induce large signals in the measuring coils.

With the pick-up coil and the sample on a line parallel to the applied field, the output of the pick-up coil is proportional to $I_{||}$, the component of magnetization parallel to the applied field, and when plotted versus field yields the standard hysteresis loop. With the coil and sample on a line perpendicular to the applied field, the output is proportional to $I_\perp$, the component of the magnetization perpendicular to the applied field. Since the torque is simply $HI_\perp$, where H is the applied field, a determination of $I_\perp$ as a function of H contains the equivalent information.

The d.c. hysteretic properties of a Permalloy film 83% Ni - 17% Fe, 1 cm. in diameter and 1000 Å thick, are displayed in Figure 33. The saturated hysteresis loop and several minor loops, obtained by plotting $I_{||}$ versus an applied field in the easy direction, are shown in Figure 33A. The step-wise variation of $I_{||}$ near the coercive field is thought to be real and is attributed to Barkhausen jumps of the magnetization. The high field loop at 10,000 oe maximum is for the same situation and is indicative of the ability to measure the film properties at large values of field. The slight decrease in $I_{||}$ at high fields is associated diamagnetic susceptibility of the glass sample substrate. Figure 33C shows $I_\perp$ versus an applied field in the hard direction after the film was first saturated in the easy direction. This result is in agreement with the 90° remanent torque curves which have been studied previously[39,48,59] in conventional torque magnetometers.
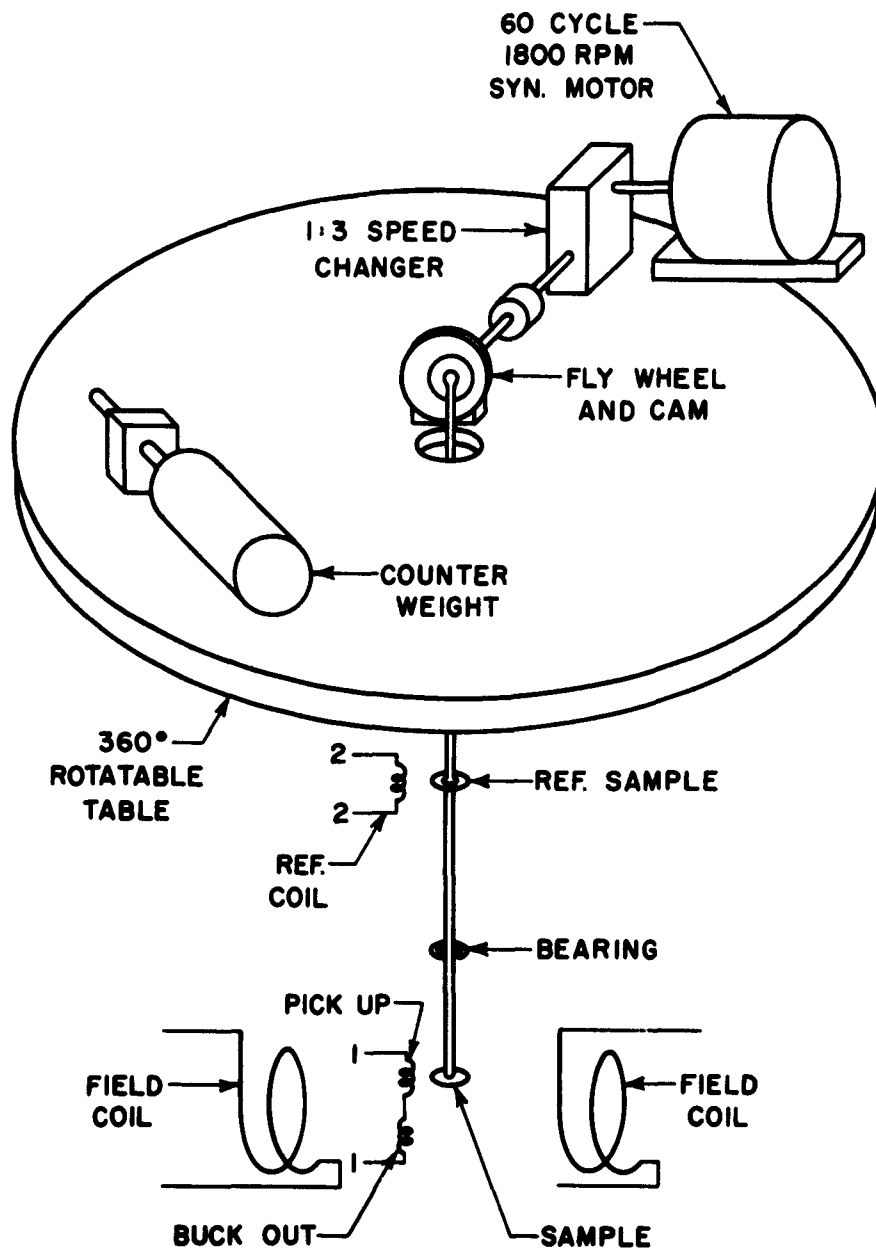
Fig. 32 - Schematic diagram of motor driven 90 cycle vibrating sample magnetometer and coil configuration.

57

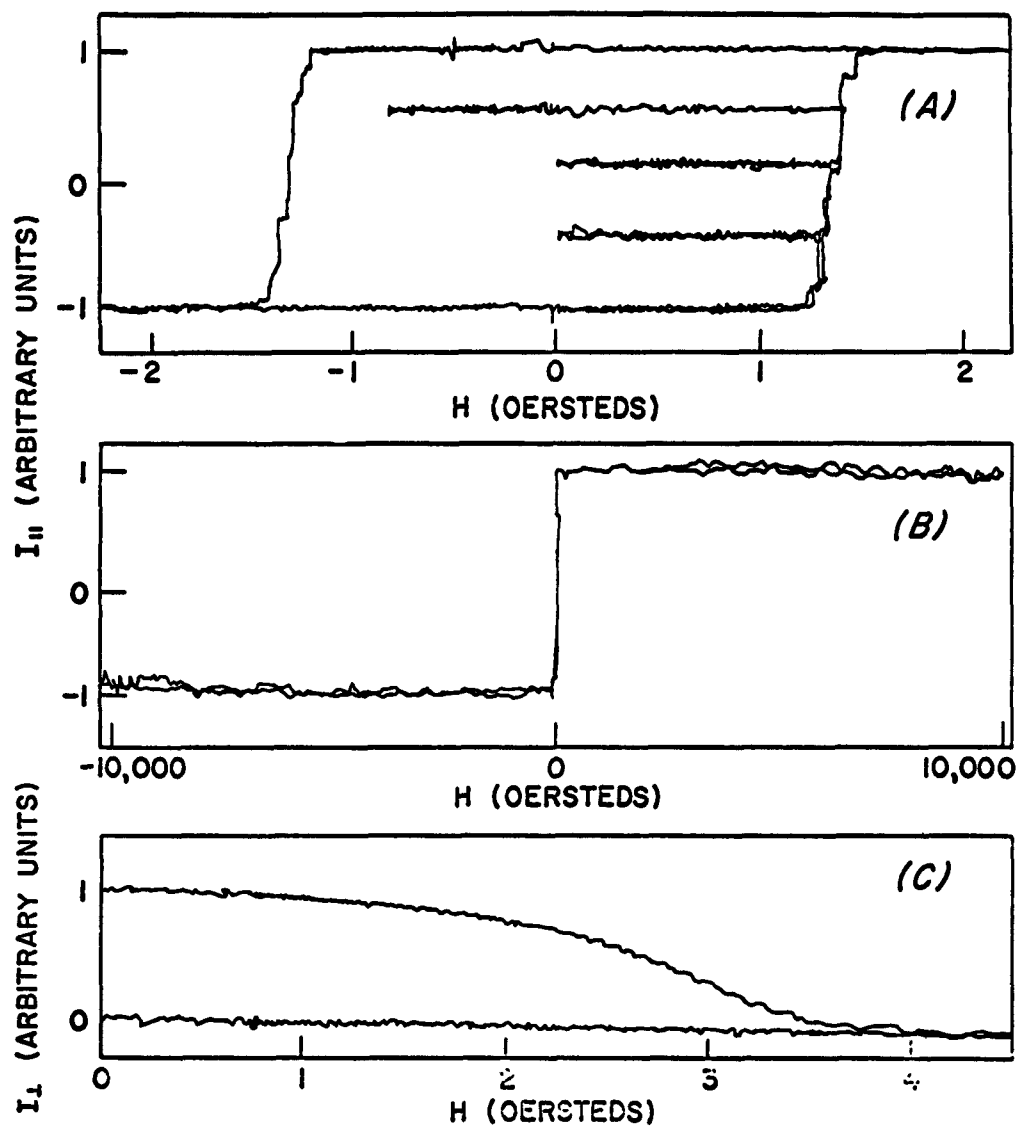Fig. 33 - Hysteretic properties of a permalloy film 83% Ni - 17% Fe, 1 cm in diameter and 1000Å thick. (A) low field $I_\parallel$ versus H; (B) high field $I_\parallel$ versus H; (C) $I_\perp$ versus H.

It is concluded that the d.c. hysteresis properties of thin magnetic films with magnetic moments as low as 10^{-3} emu can be conveniently studied using a simple vibrating sample magnetometer.

IV CONCLUSIONS

1) The degree of alignment of particles in an evaporated film is dependent upon its thickness and angle of incidence of evaporation.

2) Annealing of pseudo-monocrystalline films will result in perfect monocrystalline films exhibiting a high percentage of twinning.

3) There is evidence that perfect monocrystalline films can be grown without annealing, when they are evaporated in ultra high vacuum.

4) The angular dependence of the torque for $h_c < 0.5$ is both theoretically and experimentally straightforward. The results agree very well with the formulas derived by Shtrikman and Treves for the magnetization reversal in an infinite cylinder.

5) The angular dependence of the torque is very complex when $h_c > 0.5$. The unidirectional hysteresis observed can be understood very well if the existence of regions with negative anisotropy is assumed.

6) If the hysteresis loop in the hard direction is linear for $H > 0.5 \ H_k$, the value of H_k obtained by extrapolation to saturation will be equivalent to $2K/I_s$ where K is determined from the amplitude of the torque at high fields.

7) A dispersion in both magnitude and direction exists in the anisotropy. This can be determined by a torque method.

8) If the anisotropy field, H_k, is given by $\frac{2K}{I_s}$, which will be true for low dispersion films, the error in the torque measurement introduced by a 5° tilt is less than 10% for measuring fields less than $10H_k$.

9) The large anisotropy found in films evaporated at grazing incidence is a shape effect. This leads to a value of this anisotropy for iron to be ~ 3 times that in Permalloy.

10) Films which are shown to be single crystal by electron diffraction technique do not always possess crystalline anisotropy. This is suspected to be due to a grain size limit for single crystal behavior in electron diffraction which is lower than that size necessary for the appearance of anisotropy.

11) The d.c. hysteresis properties of thin magnetic films with magnetic moments as low as 10^{-3} e.m.u. can be conveniently studied using a simple vibrating sample magnetometer.

60

FUTURE WORK

It is recommended that further attempts to correllate the structural and magnetic properties of the films be concentrated on single crystal films. Here the structural situation is sufficiently clear and well defined so that the very slight structural effects which are able to affect the anisotropy can be detected. A comparison of single crystal films prepared at 10^{-6} mm. of Hg with those prepared at 10^{-9} mm. of Hg. would also be significant. Since NaCl is hydroscopic, other substrates e.g. CaF_2, might prove more convenient and reduce the probability of film oxidation.

These results are contained in part in the following publications

1) A. Baltz, J. Appl. Phys. 33, 1115 (1962).

2) F. R. L. Schoening and A. Baltz, J. Appl. Phys. 33, 1442 (1962).

3) A. Baltz, Rev. Sci. Inst. 33, 246 (1962).

4) A. Baltz, The World Through the Electron Microscope, Metal Edition, Vol. II (Japan).

5) W. D. Doyle, J. E. Rudisill and S. Shtrikman, J. Appl. Phys. 32, 1785 (1961).

6) W. D. Doyle, J. E. Rudisill and S. Shtrikman, Proc. of Int. Conf. on Magnetism and Crystallography, Kyoto, Japan, J. Appl. Phys. 33, 1162 (1962).

7) W. D. Doyle, J. Appl. Phys. 33, 1769 (1962).

8) P. J. Flanders and W. D. Doyle, Rev. Sci. Inst. June 1962.

9) W. D. Doyle, J. E. Rudisill and S. Shtrikman, J. Appl. Phys. 33, 1162, (1962).

REFERENCES

1. D. E. Bradley, Brit. J. Appl. Phys. $\underline{5}$, 65 (1954).

2. D. O. Smith, M. S. Cohen, G. P. Weiss, J. Appl. Phys. $\underline{31}$, 1755 (1960).

3. H. König, G. Helwig, Optik, $\underline{6}$, 111 (1950).

4. R. D. Burbank and R. D. Heidenreich Phil. Mag. $\underline{5}$, 373 (1960).

5. H. R. Thirsk and E. J. Whitmore, Trans. Faraday Soc. $\underline{36}$, 565 (1940).

6. H. Z. Göttsche, Naturforsch, $\underline{11a}$, 55 (1956).

7. H. Göttsche, Acta Cryst. $\underline{9}$, 179 (1956).

8. J. W. Matthews, Phil. Mag. $\underline{4}$, 1017 (1959).

9. V. A. Phillips, Phil. Mag. $\underline{5}$, 571 (1960).

10. P. B. Hirsch, A. Howie, and M. J. Whelan, Phil. Trans. Roy. Soc. A$\underline{252}$, 499 (1960).

11. WADD Technical Report 60-787.

12. M. S. Blois, Jr., J. Appl. Phys. $\underline{26}$, 975 (1955).

13. J. R. Mayfield, J. Appl. Phys. $\underline{30}$, 2563 (1959).

14. R. M. Bozorth, "Ferromagnetism", Van Nostrand, N. Y., 1951, p. 514.

15. E. C. Stoner and E. P. Wohlfarth, Phil. Trans. Roy. Soc. (London) $\underline{240A}$, 599 (1948).

16. E. Kondorsky, J. Phys. U. S. S. R. $\underline{2}$, 161 (1940).

17. S. Shtrikman and D. Treves, J. Phys. Radium, $\underline{20}$, 286 (1959).

18. R. M. Bozorth, op. cit., p. 109.

19. I. S. Jacobs, F. E. Luborsky, J. Appl. Phys. $\underline{28}$, 467 (1957).

20. M. Takahashi, D. Watanabe, T. Kono, and S. Ogawa, J. Phys. Soc. Japan, $\underline{15}$, 1351 (1960).

21. D. O. Smith, J. Appl. Phys. $\underline{32}$, 70S (1961).

22. L. D. Landau and E. M. Liftshitz, "Electrodynamics of Continuous Media", Addison-Wesley Publishing Company, Inc., Reading, Massachusetts, 1960.

23. Uhlig, Pickett and McNaim, Acts a Met. $\underline{7}$, 111 (1959).

REFERENCES (Continued)

24. H. Thomas, J. Appl. Phys. 33, 1117S (1962).

25. D. O. Smith, Phys. Rev. 104, 1280 (1956).

26. C. D. Olson and A. V. Pohm, J. Appl. Phys. 29 274 (1958).

27. D. O. Smith, J. Appl. Phys. 29, 264 (1958).

28. F. B. Hagedorn, J. Appl. Phys. 30, 254S, (1959).

29. M. Prutton, Brit. J. Appl. Phys. 11, 335 (1960).

30. W. D. Doyle, J. E. Rudisill, and S. Shtrikman, J. Appl. Phys. 32, 1785 (1961).

31. E. C. Crittenden, Jr., A. A. Hudimac, and R. I. Strough, Rev. Sci. Instr. 22, 872 (1959).

32. M. Takahashi, D. Watanabe, T. Kono, and S. Ogawa, J. Phys. Soc. Japan, 14, 1459 (1959); 15, 1351 (1960).

33. W. Andra, Z. Malek, W. Schuppel, and O. Stemme, Naturwissenschaften, 46, 257 (1959).

34. E. L. Boyd, IBM J. Research Develop. 4, 116 (1960).

35. R. M. Bozorth, op. Cit., p. 579.

36. P. J. Flanders, Proceedings of the Conference on Magnetism and Magnetic Materials (Boston 1957), p. 317.

37. I. S. Jacobs and F. E. Luborsky, J. Appl. Phys. 28, 467 (1957).

38. A. E. Berkowitz and P. J. Flanders, Acta Met. 8, 823 (1960).

39. G. Robinson, Proceedings of the International Conference on Magnetism and Crystallography, Kyoto, Japan.

40. M. S. Blois, J. Appl. Phys. 26, 975 (1955).

41. J. R. Mayfield, J. Appl. Phys. 30, 256S (1959).

42. W. D. Doyle, J. E. Rudisill, S. Shtrikman, J. Appl. Phys. 33, 1162S (1962).

43. P. J. Flanders (to be published).

44. R. G. Alexander, J. Appl. Phys. 30, 266S (1959).

45. K. J. Harte, J. Appl Phys. 31, 283S (1960).

REFERENCES (Conclusion)

46. F. G. West, J. Appl. Phys. 32, 290S (1961).

47. T. S. Crowther, Group Report 51-2, Lincoln Laboratory, MIT, Lexington, Massachusetts, February 1959, revised March 1960.

48. P. J. Flanders and S. Shlrikman J. Appl. Phys. 33, 216 (1962).

49. D. O. Smith, J. Appl. Phys. 30, 244S (1959).

50. T. G. Knorr, R. W. Hoffman, Phys. Rev. 113, 1039 (1959).

51. E. W. Pugh, E. L. Boyd, J. F. Freedman, I.B.M. Jour. 4, 163 (1960).

52. M. S. Cohen, J. Appl. Phys. 32, 87S (1961).

53. W. Schuppel et al, Phys. Metals and Mettalog. 8, 30 (1959).

54. V. Kambersky et al, Czech. J. Appl. Phys. B11, 171 (1961).

55. D. O. Smith, Magnetic Properties of Metals and Alloys, American Society for Metals, 1959. p. 334.

56. P. M. S. Blackett, "Lectures on Rock Magnetism", The Weizmann Science Press of Israel, 1956, pp. 99-108.

57. G. W. Van Oosterhout, Appl. Sci. Res., Section B, 6, 101, 104 (1955).

58. S. Foner, Rev. Sci. Instr. 30, 7, 548-557 (1959).

59. W. D. Doyle, J. Appl. Phys. 33, 1769 (1962).

Aeronautical Systems Division, Dir/Materials and Processes, Physics Lab, Wright-Patterson AFB, Ohio
Rpt No. WADD TR 60-787, Pt II. INVESTIGATION OF THE STRUCTURAL AND MAGNETIC PROPERTIES OF THIN FERROMAGNETIC FILMS. Final report, Mar 63, 65p. incl illus., tables, and 59 refs.
Unclassified Report

Permalloy films evaporated to normal and oblique incidence to a substance were examined by replication of their surfaces by the electron microscope. A statistical analysis of the micrographs was made. Permalloy films were epitaxially grown on NaCl and were annealed by electron bombardment in an electron microscope.
(over)

The angular dependence of the torque in Permalloy films has been studied. The results agree very well with the formulas for magnetization reversal in an infinite cylinder. Various methods of determining the anistropy have been compared and a torque technique for measuring dispersion in both magnitude and direction developed. The anistropy found in films as a function of the angle of incidence of the evaporation beam and the anistropy in epitaxially grown films is reported. The use of a vibrating sample magnetometer to determine the hysteretic properties of thin films is discussed.

1. Thin films
2. Electron microscope
3. Crystal structure
I. AFSC Project 7371, Task 737103
II. Contract AF 33 (616)-8940
III. Franklin Institute, Philadelphia, Pa.
IV. A. Baltz, W. Doyle
V. Avail fr OTS
VI. In ASTIA collection